

Pressure-temperature evolution of a Late Paleozoic paired metamorphic belt in north-central Chile (34°-35°30'S).

ARNE P. WILLNER

Institut für Geologie, Mineralogie & Geophysik, Ruhr-Universität, D-44780 Bochum, Germany; e-mail: arne.willner@ruhr-uni-bochum.de

Abstract

In the Chilean Coastal Cordillera, two units, the Western and Eastern Series, constitute coeval parts of a Late Paleozoic paired metamorphic belt dominated by siliciclastic metasediments. The Western Series also contains rocks from the upper oceanic crust and represents an accretionary prism. Omnipresent high pressure conditions are reflected by Na-Ca-amphibole and phengite in greenschist. Peak PT-conditions of 7.0-9.3 kbar, 380-420°C point to a metamorphic gradient of 11-16°C/km. Three unique occurrences of blueschist yield deviating conditions of 9.5-10.7 kbar, 350-385°C and are interpreted as relics from the lowermost part of the basal accretion zone preserving the original gradient of 9-11°C/km along the subducting slab. Pervasive ductile deformation related to basal accretion occurred near peak PT-conditions. Deformation and PT-evolution of the metapsammopelitic rocks is similar to that of the metabasites. However, a rare garnet mica-schist yields peak PT-conditions of 9.6-14.7 kbar, 390-440°C reflecting a retrograde stage after cooling from a high temperature garnet-forming stage. It is considered to be an exhumed relic from the earliest siliciclastic rocks subducted below a still hot mantle wedge. A retrograde overprint of all rock types occurred at ~300-380°C. Continuous reactions caused crystal growth and recrystallisation with abundant free water mostly under strain-free conditions. They record a pressure release of 3-4 kbar without erasing peak metamorphic mineral compositions.

The Eastern Series lacks metabasite intercalations and represents a less deformed retrowedge area. In the study area it was entirely overprinted at a uniform depth at 3 ± 0.5 kbar with temperatures progressively increasing from 400°C to 720°C towards the coeval Late Paleozoic magmatic arc batholith. The interrelated pattern of PT data permits a conceptual reconstruction of the fossil convergent margin suggesting a flat subduction angle of ~25° with continuous basal accretion at a depth of 25-40 km and a short main intrusion pulse in the magmatic arc. The latter was accompanied by the formation of a thermal dome in the retrowedge area which remained stable relative to the vertically growing accretionary prism characterized by cyclic mass flow.

KEYWORDS: *paired metamorphic belt, greenschist, blueschist, central Chile, thermobarometry*

Running title: Paired metamorphic belt in central Chile

1. INTRODUCTION

The basement of the Coastal Cordillera in Central Chile between Pichilemu and Constitución (34°-35°30'S; Fig.1) represents a type region, where metamorphic zonation was studied during the early seventies (González Bonorino 1971). This resulted in recognition of this area as a classic Pacific-rim type paired metamorphic belt (Aguirre et al. 1972, Ernst 1975). Principles and concepts were recognized here, which could be applied to most of the metamorphic basement along the Chilean Coastal Cordillera between 26° and 55°S (see Hervé 1988 for summary). This unusually long chain represents a series of fossil, deeply subducted accretionary prisms of Permocarboneous age in the north and Mesozoic age in the south that were partly associated with magmatic arcs and high-temperature metamorphic belts of variable age (Hervé 1988). These complexes were not overprinted by later collisional processes, but destructed to variable extent by processes after the end of accretion during the continuing long-term activity at the convergent margin.

The type area was revisited, because it exposes most characteristic elements for the Chilean basement. In this paper we concentrate primarily on metamorphic processes and correlate these with concomitant deformational and magmatic events. Together with an associated geochronological study (Willner et al., this volume) this should provide a basis for a more detailed conceptual model for this type of growing continental margin. Questions tackled in detail are: What partial PT paths can be deduced from different lithologies? What governs the metamorphic reaction history in the accretionary prism? Did peak pressures vary regionally and between rock types? Why is blueschist a very rare rock type in the high pressure belt? How is metamorphism related to penetrative deformation? What is the nature of the metamorphic overprint during exhumation? What is the character of metamorphism in the concomitant high temperature belt? Is it possible to reconstruct the fossil thermal structure of the paired metamorphic belt from the restricted information preserved within its rocks?

2. GEOLOGICAL SETTING AND FIELD RELATIONSHIPS

Traditionally the basement is subdivided into two metamorphic complexes representing contrasting forearc environments, the so-called Western and Eastern Series (Fig.1). This association is a basic feature of the basement that can consistently be observed throughout the Coastal Cordillera in spite of variable ages of deposition, metamorphism and deformation. The concept was introduced by

Aguirre et al. (1972) and summarized by Hervé (1988). The Western Series comprises low grade metapsammopelitic rocks with a dominating transposition foliation and greenschist intercalations, whereas the Eastern Series lacks metabasite and is represented by a less deformed, very low grade metagreywacke/-pelite sequence. While the Western Series is regarded as an accretionary prism, the Eastern Series is considered to represent the retrowedge area (Hervé 1988; Willner et al. 2000). In central Chile the Eastern Series is partly intruded by calcalkaline plutons of a late Paleozoic arc with an associated LP/HT metamorphic overprint.

In the Western Series (Fig. 1) the predominant rocks are former turbiditic deposits characterized by a penetrative, mainly subhorizontal transposition foliation with pronounced banding. This represents a second or locally a third foliation with frequent intrafolial folding of relic bands, mostly lacks kinematic indicators and represents ductile thinning. Quartz veins of dm-thickness transposed parallel to the penetrative foliation are prominent, but also deformed crosscutting quartz veins and undeformed subvertical, quartz-filled tension gashes exist. Younger subparallel shear bands with variable transport directions are rare. Stretching lineations are characteristically subparallel to the mesoscopic fold axes and mainly NW-SE-trending in the southern part of the area, but varying in the north. Frequently black postkinematic albite porphyroblasts are present, locally giving rise to spotted schists. Whereas the metapsammopelitic schists lack garnet, an exceptional garnet mica-schist occurs only in the area of Punta Sirena (Fig.1). This rock is characterized by abundant porphyroblasts of garnet of 2-10 mm size, by a brighter colour due to predominant white mica and by a coarser grain size. It forms several layers of 10 m thickness at two localities north and south of Punta Sirena.

Metabasite intercalations in the Western Series comprise only 15-20 % of the rock volume forming lenses of m to km size. Whereas these are commonly greenschist, blueschist was observed as rare lenses of 1-5 m thickness at three localities only (Fig.1: Infiernillo beach/Pichilemu, El Molino gorge/E Cahuil and gorge/NE of Iloca). Occasional green rims around these lenses are due to intensive retrograde growth of chlorite. In the greenschist lenses relic depositional features can be observed locally: At Infiernillo beach and at Punta Lobos 20-50 cm wide pillow structures are preserved with a radial set of fractures filled with calcite and amygdules towards the centre. At Infiernillo beach also relic pyroclastic structures occur: Lenticular clasts (1-10 cm) of massive dark greenschist with abundant amygdules float in a more homogeneous matrix of lighter colour richer in ferromagnesian

minerals. The structure strongly resembles former hyaloclastite. Also relatively abundant white mica-bearing metabasite might point to abundant former tuffitic deposits. According to Godoy (1986) the chemical composition of the metabasites (particularly immobile trace elements) resembles the one of MOR- or intraplate-basalts throughout the basement of the Coastal Cordillera. Zones of enhanced fluid flow are indicated by (1) layers or irregular zones of cm to m-size characterized by phase reduction (e.g. monomineralic zones of epidote or chlorite), (2) concentrations of white albite porphyroblasts and (3) veins filled with quartz, albite, locally calcite and amphibole. The structural inventory of the metabasites is similar to that of the metapsammopelitic schists. Mesoscopic folds of cm- to m-size are more prominent and amphibole is often oriented parallel to regional stretching lineation.

Several minor rock types are associated with the metabasite: (1) few serpentinite lenses of several tens of m extent, (2) several cm to m thick local layers of marble, black graphite-rich metapelite and pure quartzite (metachert, Hervé 1988) and (3) most prominent cm- to m-thick intercalations of ferruginous metasediments. The latter comprise mainly stilpnomelane-bearing schist and quartzite with partly garnet and/or concentrations of magnetite of economic value (e.g. at Punta Sirena; Fig.1) as well as cm thick layers of massive sulfide. In south-central Chile such rocks also grade into Mn-rich sediments (spessartine quartzites; "coticules") which are regarded as premetamorphic Mn- and Fe-rich hydrothermal precipitates mixed with aluminous alteration-derived material at the surface of oceanic crust (Willner et al. 2001). A similar origin is also conceivable for the ferruginous metasediments. It should be noted here that the metabasites and their associated rock types particularly represent the upper part of oceanic crust incorporated into the accretionary prism.

In the Eastern series metabasic intercalations are absent and metagreywacke/-pelite alternations prevail with occasional calcsilicate. Particularly in the central part of the exposed Eastern Series of the study area stratigraphic coherence of strata and well preserved turbiditic sedimentary structures (cross-bedding, load casts, convolute bedding, graded bedding) are observed as well as slightly E-vergent folding of bedding by up to 10 m wide chevron folds. These rocks are overprinted by a flat west-dipping second foliation which becomes a transposition foliation approaching the Western Series. Early formed quartz veins are frequent, but albite porphyroblasts are lacking. In the study area, the Eastern Series is overprinted by a HT metamorphic event. A prior evolution of its structural

inventory under very low grade conditions can only be inferred by comparison with other areas in Chile, where the HT overprint is lacking (Hervé 1988; Willner et al. 2000). Gonzalez Bonorino (1971) mapped several prograde N-S-trending metamorphic zones with a gradient towards the axis of the batholith which intrudes the Eastern Series at its eastern flank. Incipient biotite growth coincides with the western boundary of the Eastern Series. In the north of the study area garnet and oligoclase appears shortly before the staurolite isograd. The following zone is characterized by garnet, staurolite and andalusite porphyroblasts. Then sillimanite appears and the highest grade zone is characterized by a migmatitic garnet-cordierite-sillimanite-K-feldspar-gneiss. In the southern part of the study area staurolite does not appear and temperature did not overstep the andalusite-sillimanite transition. The porphyroblasts grew postkinematically after the first and second deformation. However, local slight rotation of the porphyroblasts is observed as well as occasional stretching of andalusite blasts parallel to the regional stretching lineation with quartz-filled tension gashes. This indicates that deformation continued with minor intensity after the peak of the HT event within a similar stress field as before this overprint.

At three localities (Pichilemu, E Punta Lobos, S Boyeruca; Fig.1) a N-S-striking semibrittle *mélange*-type shear zone occurs related to a late destruction of the accretionary prism. The boundary between Eastern and Western Series in the north of the study area is a brittle reverse fault (Pichilemu-Vichuquén Fault; Fig.1), which cuts the isogrades in the Eastern Series, while in the south of the study area the boundary is transitional as observed by Godoy (1970). The prominent fault is a further late deformation which caused shortening of the accretionary prism.

Tonalite, granodiorite and granite dominate in the eastern part of the study area as part of the Southern Coastal Batholith (SCB) of Permocarboneous age (Hervé et al. 1988). Granite with magmatic muscovite is frequently observed, but also granitoids containing hornblende and titanite occur. S-types granitoids seem to be abundant in the SCB in line with high $^{87}\text{Sr}/^{86}\text{Sr}$ ratios (Hervé et al. 1988). Lucassen et al. (2004) showed that isotope ratios of Nd and Pb are similar to those of the Paleozoic metasediments indicating a magmatic arc with a high crustal component. The Western Series are intruded by three isolated small bodies of biotite granite (Fig.1; from N to S the plutons of Pichilemu, Los Ciruelos and Constitución). Scattered local post-tectonic basalt dykes of dm to m thickness and few rhyotitic dykes occur throughout the area. The Eastern Series and the batholith are

unconformably overlain by Late Triassic to Lower Cretaceous marine siliciclastic sediments and volcanic rocks.

3. PETROGRAPHICAL CHARACTERISTICS OF THE WESTERN SERIES

3.1 Rock fabric

Metabasites

The assemblage of the greenschist is *amphibole-chlorite-epidote-albite-quartz±titanite±magnetite±white mica±calcite*. Amphibole, chlorite and white mica (0.05-0.2 mm) are oriented parallel to the penetrative foliation, but crosscutting grains are frequent. The recrystallized amphibole is always euhedral, forms up to 2 mm long needles and is strongly zoned displaying bluish cores grading into green rims. Faint internal crenulation with recrystallized hinge zones can be detected within the dominant foliation. Epidote occurs as euhedral, optically zoned crystals of 0.1 mm size crosscutting the fabric. Epidote and chlorite can continuously replace the existing assemblage until monomineralic layers are formed. Titanite forms small pods or trails of tiny anhedral grains (0.01-0.04 mm) parallel to the foliation with some relic crenulation hinges or larger euhedral recrystallized grains (0.1 mm). Quartz, albite and/or calcite form small polygonal aggregates or crosscutting veinlets including all minerals of the matrix assemblage. Occasional anhedral albite porphyroblasts (0.1-0.5 mm) with internal trails of epidote and amphibole always grew after formation of the predominant foliation and across relic crenulation hinges. They may be rotated in rare sheared rocks. Opaque phases are pyrite or magnetite which grew as large euhedral recrystallized grains (0.5-1 mm). Clinopyroxene (0.1-0.5 mm) is an ubiquitous relic of the protolith assemblage. It often has irregular grain boundaries due to replacement by surrounding minerals. In some cases, large clinopyroxene crystals still display its original euhedral outline as former phenocrysts. In rare sheared rocks the mineral shows brittle deformation and rotation. Further relic fabric are occasional amygdales (1-5 mm size) filled with albite and/or calcite. The amygdales are slightly flattened in more strongly deformed areas.

The assemblage of the rare blueschist is *blue amphibole-chlorite-epidote-albite-quartz±white mica±titanite±magnetite±calcite*. Banding at mm to cm scale is represented by dark bands of weakly oriented euhedral amphibole, chlorite, epidote and white mica (0.05-0.2 mm) alternating with bright bimineralic bands (amphibole-quartz, amphibole-epidote, amphibole-chlorite) or monomineralic

strings (amphibole, chlorite, titanite, white mica or epidote). Also crenulation of a relic foliation can be observed within the bands with oriented minerals recrystallizing in the crenulation hinges. Epidote and amphibole are optically zoned. Green amphibole overgrew blue amphibole along the rims. One sample (12544) contains relic clinopyroxene (0.5 mm). Unoriented euhedral albite crystals of similar size occur near the clinopyroxene crystals suggesting a further magmatic relic. Quartz-albite veinlets with some blue amphibole occur parallel to the bands or cut across.

At four localities serpentinite lenses of 10 m scale are associated with the greenschist. Clinopyroxene occurs as the only relic phase forming a network of mainly 0.5 mm sized crystals surrounding entirely replaced phases with partly euhedral outline. Replacement minerals are mainly antigorite and minor tremolite and chlorite as well as exsolutions of magnetite. The original fabric resembles cumulates. Godoy & Kato 1990 also described pyroxene relics and abundant layered magnetite concentrations in serpentinite from south-central Chile pointing to a similar origin.

Ferruginous metasediments

The three recognized types of iron-rich metasediments - stilpnomelane quartzite, stilpnomelane schist and magnetite-stilpnomelane rocks - can grade into each other and into the associated greenschist. The general assemblage is *magnetite-stilpnomelane-amphibole-garnet-quartz-albite±white mica±chlorite±epidote*.

Stilpnomelane (0.1-0.3 mm) grew unoriented in a polygonal quartz fabric in stilpnomelane quartzite with occasional chlorite, white mica, amphibole and rare trails of tiny, optically zoned garnet (0.01-0.05 mm) or forms nearly monomineralic layers of oriented and crosscutting crystals (0.05-0.5 mm) in stilpnomelane schist. Occasional unoriented porphyroblasts of albite or magnetite (0.4-0.8 mm) grew across stilpnomelane. The rocks are mostly banded at mm-scale containing some rootless isoclinal intrafolial microfolds with recrystallized fold hinges. Monomineralic pods of magnetite, stilpnomelane, garnet (0.01-0.05 mm) or epidote with a polygonal fabric occur.

Metapsammopelitic schist

The general assemblage of the monotonous metapsammopelitic schist is *quartz-albite-white mica-chlorite-ilmenite±magnetite±epidote*. The heavy mineral spectrum is reduced to zircon, apatite and tourmaline. Prominent is a banding of alternating mm-thick quartz- and phyllosilicate-rich bands. Quartz and albite (0.05-0.30 mm) form a polygonal fabric without relics of former detrital or oriented

grains, but with local subgrain formation and sutured grain boundaries indicating late continuous deformation. White mica and chlorite (0.1-0.3 mm) are intensively intergrown showing a relic orientation. Crenulation hinges of various generations (F_2 , F_3) are prominent, but the phyllosilicates are recrystallised in the hinges with frequent growth of cross mica. Albite porphyroblasts (0.5-2 mm) are a late, mostly unoriented phase and an intrinsic feature of the metapsammopelitic schist overgrowing fold hinges of all generations (F_2 , F_3). They are often macroscopically black due to internal inclusion trails of graphite which redraw relic crenulation hinges. The porphyroblasts are bound to the phyllosilicate-rich bands growing at the expense of white mica. In some cases they can completely replace white mica forming bands of albite. The porphyroblasts are euhedral or partly anhedral due to incomplete development of the crystals or to late pressure solution at the rims. Apart from this feature also local slight rotation of the porphyroblasts indicates continuing weak deformation after growth of the porphyroblasts.

The assemblage of the unusual garnet mica-schist at Punta Sirena is *garnet-quartz-albite-white mica-chlorite-epidote-titanite* \pm *ilmenite* \pm *rutile*. Garnet porphyroblasts range from 1-10 mm size with internal sigmoidal trails of titanite, ilmenite or quartz (0.01-0.05 mm). Near the rims the garnet overgrew a polygonal fabric of coarser quartz (0.05-0.3 mm) similar to that of the surrounding matrix. The grains are euhedral or partly strongly replaced at the rims by white mica and chlorite, in some samples also along cracks by chlorite and epidote. Dominant white mica and minor chlorite (0.2-0.5 mm) form two foliations within a matrix of polygonal quartz and albite. The phyllosilicates recrystallize in crenulation hinges and crosscutting grains are abundant. An early white mica occurs as inclusions in garnet and titanite. Subhedral grains of unoriented epidote (0.05-0.10 mm) are abundant in the foliation planes. Titanite forms euhedral unoriented crystals of 0.1-0.5 mm size in the matrix, occasionally enclosing round rutile. Albite displays prominent unoriented porphyroblasts (0.2-0.5 mm) enclosing trails of graphite, epidote, white mica, titanite or garnet. Some garnet mica-schist samples show a prominent orientation of the phyllosilicates parallel to the prevailing foliation. Here porphyroblasts of garnet, albite and titanite are strongly rotated indicating a late localized non-coaxial deformation.

3.2. Mineral Chemistry

Mineral analyses were achieved with a Cameca SX 50 microprobe at Ruhr-Universität Bochum, Germany. Operating conditions were an acceleration voltage of 15 kV, a beam current of 15 nA, 20s counting time per element on the peak and on the background and a defocussed beam of 8 μm diameter in order to avoid loss of alkalis in micas, feldspars and amphiboles. Standards used were synthetic pyrope (Si, Al, Mg), rutile (Ti), glass of andradite composition (Ca, Fe), jadeite (Na), K-bearing glass (K), topaz (F), Ba-silicate glass (Ba; $L\alpha$). The PAP procedure was used for matrix correction. Representative analyses and structural formulae of minerals used for PT-calculations, together with the calculation procedure of the structural formulae, are presented in Table 1. Further analyses are provided in an extended table in the electronic deposit of the journal and upon request to the author. Element distribution maps were simultaneously produced for three elements by stepwise scanning over rectangular areas. Abbreviations for minerals and mineral components used throughout the text follow Kretz (1983), if not indicated otherwise.

Clinopyroxene

The clinopyroxene is augite of magmatic origin and hence the only abundant relic of the protolith of some metabasites. Its composition (Table 1) varies strongly: diopside₃₅₋₆₈, hedenbergite₁₋₁₅, orthopyroxene₀₋₁₃, acmite₀₋₂₈, tschermak-component₀₋₂₈ with notable traces of Ti (0.01-0.06 apfu) and Cr (0.00-0.03 apfu). The composition follows a similar trend within all samples which is identical to the compositional range of clinopyroxene in the field assigned to “within-plate alkali basalt” of the MnO-TiO₂-Na₂O variation diagram (Nisbet & Pearce 1977; Fig.2). This comparison is corroborated by relatively low SiO₂ (44.7-45.9 wt%) as well as relatively high Na₂O (0.2-2.8 wt%), Al₂O₃ (2.1-6.9 wt%) and TiO₂ (0.5-2.2 wt %). Most Ca+Na-contents exceed 0.9, which is characteristic for alkaline rocks (Leterrier et al. 1982). The relic clinopyroxene from serpentinite sample F541 also follows the described trend implying that it presumably represents former cumulates within the oceanic crust. Summarizing, part of the accreted oceanic crust is most likely represented by ocean island basalts.

Garnet

Garnet in the Western Series is restricted to the unusual garnet mica-schist and the ferruginous metasediments. The garnet mica-schist contains a grossular-rich garnet with the compositional range almandine_{0.47-0.76}, grossular_{0.14-0.34}, spessartine_{0.01-0.21}, pyrope_{0.02-0.09} (X_{Mg} 0.02-0.13, Ti \leq 0.04; Table 1). Zoning is typically prograde and bell-shaped with an increase in Ca and Mg and a decrease in Mn, Fe²⁺, Fe³⁺, and Ti from core to rim. Zonation of Ca is distinctly oscillatory.

In the ferruginous metasediments, the garnet is Mn- and Ca-rich with the compositional range almandine_{0.14-0.47}, spessartine_{0.27-0.56}, grossular_{0.18-0.26}, pyrope_{0.01-0.03}, uwarovite_{0.06-0.07}, andradite_{0.01-0.04} (X_{Mg} 0.06-0.12, $Ti \leq 0.04$ apfu). These compositions are rather similar to that of garnet in spessartine quartzite (coticule) in other parts of the basement, which have a premetamorphic hydrothermal origin (Willner et al. 2001). Zonation is prograde and bell-shaped with an increase in Ca, X_{Mg} , Mg and Fe^{2+} and a decrease in Mn and Fe^{3+} from core to rim.

Amphibole

At the three blueschist localities (see above; Fig.1) Na-amphibole varies from glaucophane to magnesioriebeckite composition (Fig.3a; Table 1; nomenclature after Leake et al. 1997) and covers a wide continuous range of $X_{Fe^{3+}}$ (0.21-1.00) and Na^B ($= Na^{M4}=1.51-1.93$ apfu) with more restricted X_{Mg} (0.52-0.85). Towards the rims the Na-amphibole continuously grades into NaCa-amphibole and actinolite (Fig.3b; Fig.4). The NaCa-amphibole is winchite (Na^B 0.50-1.49 apfu, $Na^A < 0.28$ apfu, X_{Mg} 0.63-0.93, $X_{Fe^{3+}}$ 0.29-1.00, Si 7.43-8.00 apfu), which is partly ferrian (Fe^{3+} 0.75-1.74 apfu) pointing to a relatively oxidized environment. At the outer rims actinolite occurs (Na^B 0.21-0.49 apfu, $Na^A < 0.21$ apfu, X_{Mg} 0.68-0.79, $X_{Fe^{3+}}$ 0.63-0.98, Si 7.45-7.88 apfu).

In the greenschist and the ferruginous metasediments, amphibole mostly grades from NaCa-amphibole to Ca-amphibole or is Ca-amphibole with a high Na^B -content (Fig.3d; Table 1). This variation also corresponds to high Na^B in the core decreasing towards the rims. The NaCa-amphibole (Na^B 0.50-0.88 apfu, Na^A 0.00-0.31, X_{Mg} 0.40-0.82, $X_{Fe^{3+}}$ 0.60-0.97) includes winchite (Si 7.50-7.93 apfu) and barroisite (Si 6.64-7.48 apfu). Barroisite is partly ferribarroisite (Fe^{3+} 1.23-2.00 apfu) in the ferruginous metasediments. The Ca-amphibole (Na^B 0.02-0.49 apfu, Na^A 0.00-0.39, X_{Mg} 0.58-0.86, $X_{Fe^{3+}}$ 0.30-1.00) ranges gradually from actinolite (Si 7.58-7.93 apfu) to magnesiohornblende (Si 7.00-7.48 apfu). It is notable that - at a given Na^B -content - the total R^{3+} -content in the amphiboles of the greenschist is considerably higher than in those of the blueschist (Fig. 3b, d; except sample M3404). This may be due to a higher tschermak substitution in the amphiboles of the greenschist leading part to barroisite and magnesiohornblende compositions.

The overall compositional variation of amphibole during continuous grain growth as well as between peak metamorphic compositions of different samples shows complete transitions between Ca- and Na-amphibole suggesting that no miscibility gap exists between Na- and Ca-amphiboles at the given

conditions and compositions. Amphibole compositions can be plotted in terms of “actinolite, glaucophane and riebeckite components” (Fig.3c, e) showing complete solid-solution between Fe-rich Ca- and Na-amphiboles. The remaining possible solid-solution gap between Mg-rich actinolite and glaucophane must be smaller than the one calculated by Massonne (1995) for 300°C indicating amphibole growth at $T > 300^{\circ}\text{C}$.

White mica

White mica of phengite composition occurs in all rock types (Table 1). Si contents are highest in the blueschist (3.33-3.53 apfu) with a variation of 0.10-0.15 apfu in single samples, while the range is wider in the greenschist (3.14-3.5 apfu) with mostly lower maximum content and a similar range in single samples (Fig.5). Si-contents are still lower in the metapsammopelites (3.10-3.30 apfu), but also in the garnet mica-schist (3.2-3.36 apfu). Ti- and Na-contents are very low in all rock types (<0.05 apfu). Most compositions plot below the ideal Tschermak-substitution line in Fig.5 owing to partial substitution of Al by Fe^{3+} and some di/trioctahedral substitution. Fe^{3+} -contents were estimated normalizing the sum of cations on the octahedral site to 2.05 apfu (see Massonne 1995). This is due to a restriction of the di/trioctahedral substitution experimentally detected by Massonne & Schreyer (1986) for white mica with variable Si-contents. Calculated Fe^{3+} -contents are highest in the magnetite-rich ferruginous metasediments (0.17-0.36 apfu) and in the metabasites (<0.32 apfu) which also contain Fe^{3+} -rich amphibole. No Fe^{3+} was estimated in the white mica of the metapsammopelites. In each metabasite sample there is a strong negative correlation of Si with Fe^{3+} that seems to be enriched in the Si-poor rims of phengite grains

No unambiguous pattern of chemical zonation could be detected, but lower values of Si are mostly measured near the rims. Only in the ferruginous metasediments notable Ba-contents exist (0.03-0.07 apfu) presumably representing a premetamorphic hydrothermal component. Relic prograde phengite is only observed in the garnet mica-schist as inclusions in garnet and titanite which shows slight chemical difference (Si 3.2-3.25 apfu., X_{Mg} 0.64-0.7, Na 0.07-0.12 apfu., Ti 0.15-0.3 apfu) compared to the matrix white mica (Si 3.24-3.36, X_{Mg} 0.5-0.7, Na 0.02-0.07, Ti 0.005-0.01).

Chlorite, Titanite, Epidote, Stilnomelane

Chlorite compositions in the metabasites vary within a similar range (Si = 2.55-3.10 apfu; X_{Mg} = 0.52-0.68). Among minor elements only Mn has a notable abundance (0.02-0.17 apfu). Chlorite in

metapsammopelitic rocks has partly lower Si-contents (2.52-2.74 apfu) and X_{Mg} (0.31-0.55) than in the metabasites.

Titanite is a prominent accessory phase in metabasites and in the garnet mica-schist with a $Ca(Al,Fe^{3+})SiO_4(F,OH)$ -component between 4 and 52 mole%. Notable contents of F (0.02-0.59 wt %), Al (0.03-0.46 apfu) and Fe^{3+} (0.01-0.22 apfu) are observed. The Fe^{3+} -content of *epidote* varies widely in different samples (0.44-0.99 apfu), but generally an increase is observed from core to rim. *Stilpnomelane* is the rock-forming mineral in the ferruginous metasediments with notable contents of Mn (0.19-0.40 apfu) and Na (0.11-0.23 apfu).

4. PETROGRAPHICAL CHARACTERISTICS OF THE EASTERN SERIES

Apart from very rare calcsilicate rocks, the Eastern Series are lithologically extremely homogeneous and assemblages, fabric as well as mineral chemistry change in response to the zonation of the high temperature metamorphic overprint.

Within the biotite zone the main assemblage is *biotite-chlorite-muscovite-quartz-plagioclase±ilmenite*. The first biotite grew at the expense of white mica and chlorite either as mimetic growth along oriented phyllosilicates or as porphyroblasts of 0.05-0.30 mm size. A polygonal fabric of quartz and plagioclase is prominent. In the biotite zone white mica is muscovite only (Si 3.00-3.16 apfu, Na 0.05-0.15 apfu, Ti 0.01 apfu), plagioclase is oligoclase (15-19 mole % anorthite), whereas biotite (X_{Mg} 0.32-0.34, Ti 0.1 apfu) and chlorite (Si 2.5-2.75 apfu, X_{Mg} 0.34-0.36, Mn 0.04-0.07 apfu) are Fe-rich (Table 1). Compositional variation within and among samples is low.

A staurolite-andalusite zone is only observed in the north of the study area. Two main assemblages are: *garnet-biotite-muscovite-plagioclase-quartz±staurolite±ilmenite* and *andalusite-biotite-muscovite-plagioclase-quartz±staurolite±ilmenite*. Although porphyroblasts of garnet, biotite, staurolite and andalusite grew post-kinematically with respect to the penetrative foliation, slight rotation is observed locally indicating continuing deformation with waning intensity after the peak of HT-metamorphism. Staurolite porphyroblasts (1-2 mm) are euhedral with tiny inclusions of quartz and biotite. At the rims slight replacement by muscovite, chlorite and ilmenite is observed. Small euhedral garnet porphyroblasts (0.1-0.3 mm) are nearly devoid of inclusions. The size of the prominent andalusite porphyroblasts ranges from 0.1 to several cm. Frequently partial replacement by serizite and chlorite

occurs indicating very low temperature alteration. Also quartz-rich calcsilicate rocks are locally observed containing the assemblage *garnet-clinopyroxene-quartz-plagioclase-titanite*.

In the south of the study area medium grade conditions are represented by an andalusite-sillimanite zone as the highest grade without appearance of staurolite. However, some poikilitic cordierite in the matrix has been described by Gana & Hervé (1981). Andalusite porphyroblasts are only of 1-2 mm size, but locally abundant. In the eastern part of the zone fibrolite appears replacing andalusite at the rims.

Medium grade schists are characterized by muscovite (Table 1) with an increased paragonite component Si 3.00-3.09 apfu, Na 0.20-0.27 apfu, Ti 0.01-0.017 apfu), oligoclase (19-25 mole % anorthite), Mg-rich biotite (X_{Mg} 0.28-0.35, Ti 0.09-0.11 apfu) and staurolite with traces of Mn and Zn (X_{Mg} 0.12-0.17, Mn 0.022-0.035 apfu, Zn 0.021-0.029 apfu). Garnet composition is almandine_{0.73-0.89}, pyrope_{0.05-0.08}, spessartine_{0.03-0.19}, grossular_{0.02-0.02} (X_{Mg} 0.06-0.12, Ti \leq 0.04 apfu). Its zonation is bell-shaped with decreasing Mn, Ca, Ti and increasing Mg, Fe from core to rim. X_{Mg} remains constant.

In the highest grade zone of the northern study area a migmatitic gneiss with the assemblage *garnet-cordierite-sillimanite-K-feldspar-plagioclase-quartz* occurs. Garnet forms prominent anhedral porphyroblasts (0.5-1.0 cm) with inclusions of quartz, biotite, sillimanite particularly near the rims. Garnet composition (Table 1) is almandine_{0.79-0.81}, pyrope_{0.12-0.15}, spessartine_{0.02-0.03}, grossular_{0.02-0.04} (X_{Mg} 0.13-0.16, Ti \leq 0.04 apfu). The garnet is internally unzoned. Quartz and plagioclase (19-25 mole % anorthite) show secondary recrystallisation of large crystals (0.3-0.8 mm) at the expense of smaller ones with abundant inclusions of biotite, fibrolite and apatite. Cordierite (X_{Mg} 0.55-0.58, Na 0.06-0.11 apfu; Mn 0.007-0.015 a.p.f.u) with inclusions of biotite and fibrolite is intergrown with quartz and plagioclase. Two generations of sillimanite are present: Fibrolite forms prominent unoriented nodes and bands replacing biotite at its contact. Prismatic sillimanite (0.5 mm) replacing fibrolite and biotite form aggregates of cm-size. Ti-rich biotite grains (0.2-1 mm; X_{Mg} 0.38-0.45, Ti 0.13-0.21 apfu) grew entirely unoriented. Local late retrograde muscovite grew across sillimanite. The gneiss contains local migmatitic leucosomes of granitic composition.

5. METAMORPHIC EVOLUTION OF THE WESTERN SERIES

5.1 Phase relationships and reaction history

To visualize the approximate PT-fields of high variance blueschist and greenschist facies assemblages, pseudosections were calculated in the system $K_2O-Na_2O-CaO-TiO_2-Fe_2O_3-FeO-MgO-Al_2O_3-SiO_2-H_2O$ from the whole rock composition of two typical white mica-bearing greenschist and blueschist samples as well as for three metapsammopelitic samples (Fig.6; see also for chemical analyses). For calculating the equilibrium assemblages and respective mineral compositions, the Gibbs free energy minimization procedure was applied using the DEKAP code developed by Gerya et al. (2001). This approach is based on an algorithm suggested by de Capitani & Brown (1987). The calculation of the petrogenetic grid was performed with a resolution of 5 K and 100 bar for T and P, respectively. Calculations involved the entire thermodynamic data set for minerals and aqueous fluids of Holland & Powell (1998). References to applied mixing models consistent with this database are listed in Table 2.

In the calculated pseudosections of the blue- and greenschist samples, which have no marked chemical differences (Fig.6 a, b) a similar narrow transitional field exists between the blueschist and greenschist assemblages between 300-400°C at ~5-7 kbar up to 6-8.5 kbar. Two amphiboles are predicted to coexist in this transitional field. This contrasts the observation made in section 3.2 that a complete compositional transition exists between Na- and Ca-amphiboles within the studied samples. The transition between the facies stability fields is rather represented by the NaCa-amphiboles winchite and barroisite, which are common in all metabasite. Hence the predicted coexistence of two amphiboles in the pseudosections must be due to the used activity models for amphiboles which imply a too wide mixability gap. Nevertheless the minimum pressure for blueschist assemblages at 7.8-8.8 kbar, 300-400°C is equivalent in both pseudosections. This predicts that there is a pressure difference between the recorded peak assemblages of the blue- and greenschist samples. Lawsonite that is not observed in our samples appears at pressures above 9-11 kbar at 300-350°C. This can be taken as a lower temperature limit for the studied epidote blueschist facies assemblages. At the highest temperature limit, a transitional field to the albite amphibolite facies may already appear at 430°C. In the greenschist assemblages biotite would be stable at $T > 400^\circ\text{C}$ and $P < 4-5$ kbar.

A typical pseudosection for the metapsammopelites (Fig.6c) shows that their common assemblage white mica-chlorite-quartz-albite±epidote is stable over a very wide PT-field including greenschist, epidote blueschist and albite-epidote amphibolite facies. Lawsonite is predicted already at 9-11 kbar and 300-350°C representing a good lower temperature limit. Garnet in the Western Series is restricted only to very Mn-rich assemblages like the ferruginous metasediments and it is thus stabilized to low temperature by high Mn-contents. An exception is the Ca-rich garnet mica-schist of Punta Sirena, where garnet is predicted to be stable above 10-11 kbar. However, in the absence of omphacite temperatures should have exceeded ~450-500°C (Fig.6d). The calculated composition of the high pressure garnet (e.g. at 11 kbar/550°C: almandine_{0.661}, grossular_{0.241}, pyrope_{0.098}) corresponds well with the measured one (see section 3.2).

Thorough recrystallisation of quartz within the penetratively deformed rocks lacking any visible distinction between clastic and recrystallized grains in the metapsammopelites indicates maximum temperatures above 350°C (Brix et al. 2002). The pumpellyite-breakdown reaction marking the boundary between pumpellyite-actinolite and greenschist facies (Evans 1990; here calculated for mean compositions; method I, Table 2) at 300-350°C/>5 kbar (Fig.8b), was well overstepped in the entire study area. Also retrograde pumpellyite did not form indicating that retrograde metamorphic reactions appear to have ceased before cooling through 300°C. On the other hand, four localities of ferruginous metasediments (associated with blue- and greenschist) contain the assemblage stilpnomelane-white mica (Fig.1) proving that temperatures did not exceed stilpnomelane break-down to biotite coexisting with phengite and quartz (Massonne & Szpurka 1997; here calculated for mean compositions; method I, Table 2) at ~350-400°C/>5 (Fig.8a). Hence the evolution of most rocks of the study area was apparently restricted to a rather narrow temperature range. Maximum pressure is limited by the presence of pure albite in all rock types to below 10.5-12.5 kbar at 300-400°C.

The reaction history leading to the omnipresent conspicuous retrograde zoning in amphibole and other hydrous phases (white mica, chlorite, epidote) appears to be governed by the presence of a free interstitial hydrous fluid phase. Abundant growth of postkinematic late albite porphyroblasts and different generations of late quartz-filled veins cutting the pervasive foliation are visible expressions for the presence of free fluids on the entire retrograde path (see section 2). However, is external fluid influx necessary, considering the common assumption that water released during prograde

dehydration left the system? Pressure-sensitive multivariant reactions at the blueschist/greenschist facies transition that are used for geobarometry below (see section 5.2) have partly water as reactant on the high pressure side like reaction E6 (see Table 3), but also on the low pressure side (see reaction 5, Table 3). This means that water can be consumed or released during continuous retrograde decompression reactions. The calculated pseudosections allow to quantify the change in the amount of free water relative to the bulk water content of the system with changing PT-conditions (Fig.7), assuming that reactions are instantaneous and complete and the water content of the rock was the total water content of the system. Considering PT-changes from 400°C, 8-10 kbar to 350°, 5kbar (simulating the partial PT-path derived in section 5.2) the changes in $X_{\text{free water}}/X_{\text{bulk water}}$ are negative for greenschist sample 95CH24 (consumption of free water), but positive for blueschist sample 95CH11 and the metapsammopelitic sample 98CH32 (release of free water). This predicts that with continuous reaction during decompression at low grade conditions (either isothermally or with slight cooling), the amount of free water might increase in many cases so that no external water is required for reactions to proceed. A limited amount of steadily available free water will favour localized equilibrium over short distance during continuous mineral growth with activities of elements in the fluid always buffered.

5.2 Geothermobarometry

For quantification of the PT-conditions for equilibration stages along the PT-path, local equilibria with multivariant reactions were calculated using mineral compositions of phases in close contact. Multivariant equilibria calculations were undertaken mainly using the Ge0calc-software of Brown et al. (1989) and derivations (TWQ) with the thermodynamic data set of Berman (1988) supplemented by further compatible data and activity models (Table 2). A list of the calculated reactions is given in Table 3. Results are plotted in Fig. 8.

Metabasite

Due to a high number of reliable components available for calculations, good geothermobarometric results were obtained for the low-variance assemblage amphibole-white mica-chlorite-epidote-quartz-albite. Invariant points were calculated using the water-independent multivariant reactions E1-E4 (Table 2). Including water as a further phase, 9 additional reactions were calculated. However, these relatively flat water-dependent reactions are not only sensitive to minor changes in (unknown) water

activity, but are much more dependent on the activity of the clinozoisite component than the water-independent ones. Thus their use as a further check for equilibrium conditions is limited, although closest coincidence of all possible invariant points was always approached. For blueschist samples lacking chlorite, the water-dependent reaction E5 was used as a barometer, for greenschist lacking white mica, the water-dependent reaction E6 was calculated.

The two generations of amphibole in the two different metabasite rock types reflect two stages of equilibration along a partial PT-path, a peak metamorphic stage I and a retrograde stage II. Calculations of the stage I-conditions result in a range of PT-data (invariant points) of 9.5-10.7 kbar, 350-385°C for the blueschist and 7.0-9.3 kbar, 380-420°C for the greenschist (Fig.8). The temperature range for the latter was independently corroborated by conventional Fe-Mg exchange thermometry with rims of garnet-amphibole pairs (*Graham & Powell 1984*) in two magnetite-stilpnomelane rocks (samples 95CH25, 98CH25). The scatter presumably represents continuous equilibration around peak PT-conditions during the late prograde and early retrograde PT-path that could not be resolved in detail in the present case, but also differences in peak pressure between greenschist samples are likely. Calculations of the stage II-conditions yielded a range of PT-data of 6.0-7.7 kbar, 290-345°C for the blueschist and 4.4-7.2 kbar, 315-380°C for the greenschist (Fig.8) thus indicating pressure release with slight cooling. The slight temperature difference between the paths of the blueschist and greenschist presumably concurs with a generally higher Tschermaks substitution in the amphiboles of the greenschist (see section 3.2).

No regional trend in the distribution of peak pressures occurs (Fig.1), but a significant peak pressure difference between both metabasite types results as predicted from the pseudosections. It was often argued that the very rare blueschist assemblages were principal relics of HP/HT-conditions generally completely erased by pervasive retrograde greenschist overprint (e.g. Kato 1985; Martin et al. 1999). Here peak PT compositions of solid solution phases are regarded as preserved in most rock types for the following reasons:

- Relic magmatic clinopyroxene phenocrysts are replaced by Na-, CaNa- or Ca-amphibole in different rock types. It seems unlikely that a premetamorphic phase is preserved, but not the peak metamorphic amphibole.

- Pervasive overprint erasing all relic compositions could be driven by abundant external fluid influx, but this should lead to phase reduction. Such metasomatic effects are frequently observed, but not predominant in the metabasite lenses, where low-variance assemblages are also common. It was shown above (section 5.1) that major external fluid infiltration is unlikely for most studied rocks.

Metapsammopelite

For the high variance assemblage present in most metapsammopelitic rocks, so far only the approach by Vidal & Parra (2001) and Parra et al. (2002a, b) using coexisting chlorite-phengite equilibria was shown to yield consistent results being tested especially for metapelites in similar HP-LT terranes. This approach (method 2; table 2) is based on thermodynamic solution models involving the tschermak, di/trioctahedral and pyrophyllitic substitutions. Application of this approach to the metapsammopelitic rocks of the study area is, however, restricted only to the water-independent multivariant equilibria E7-E9 and E3. All analysed iron is assumed to be ferrous in this approach. Other possible end members with contents in chlorite and mica of less than 5 % (e.g. sudoite, pyrophyllite) could not be considered because of the high uncertainty of their activity in these phases. For two metapsammopelitic schist samples a range of data for local equilibria of 4-9.6 kbar, 355-435 results suggesting similar peak PT-conditions and decompressional overprint as in the greenschist. Hence a comparable evolution for both rock types is inferred (Fig.8).

In contrast, the garnet mica-schist yields deviating results. Multiple tests with available multivariant reactions and conventional thermometers involving garnet do not yield any reasonable results and show that garnet is not in equilibrium with white mica or chlorite. This concurs with the observation that chlorite, white mica and epidote replace garnet at its rims. Evidently the matrix assemblage around garnet is a second retrograde one. Phengite inclusions in garnet, albite and titanite have different compositions than matrix white micas (see section 3.2) and are prograde. Considering the results from the pseudosections (see section 5.1), $P > 10-11$ kbar and $T > \sim 450-500^\circ$ must have been realized to produce the garnet during an older higher temperature stage I. Chlorite-phengite equilibria of coexisting pairs in the matrix indicate conditions of $390-440^\circ\text{C}$, 9.6-14.7 kbar (method 2; table 2). The results of this retrograde stage II partly appear to be at too high pressure, because the upper stability of albite should have been overstepped and no jadeite is observed. Nevertheless they still indicate significantly higher PT-conditions than in the metapsammopelites and the greenschist of the

study area (Fig.8). Relation between stages I and II suggest a presumable isobaric cooling path at ~12-13 kbar. The garnet mica-schist is very similar to a garnet mica-schist associated with a garnet amphibolite in the Western Series of south-central Chile (Willner et al. 2004), which yielded an anticlockwise PT-path and highest regional PT conditions. The analogy corroborates the unusual evolution of the garnet mica-schist. Similar to the analogue from south-central Chile, also the garnet mica-schist studied here yields an age related to stage II that is significantly older than the ages of the peak of metamorphism in the area (Willner et al., this volume).

6. METAMORPHIC EVOLUTION OF THE EASTERN SERIES

The interpretation of the HT-metamorphic sequence and phase relationships in the Eastern Series is straight forward (Fig.9). The zonation and sequence of mapped assemblages indicate progressive increase in grade from upper greenschist facies to granulite facies suggesting a classic “Abakuma-type” sequence at pressures below the aluminosilicate tripel point. The sequence starts with formation of biotite, passes the staurolite-in-reaction in the andalusite stability field and the staurolite-quartz-muscovite-out reaction in the sillimanite stability field and ends with first anatectic melts. Breakdown of muscovite + quartz in the sillimanite field before reaching the wet granite solidus indicates a pressure below 3.6 kbar (intersection of the muscovite + quartz breakdown and wet granite solidus curves). This is consistent with the position of the univariant reaction $Bt + Sil + Qtz = Grt + Cord + Kfs + H_2O$ of the KFMASH-system (Spear & Cheney 1989), which is recorded by the highest grade assemblage.

Geothermobarometry is consistent with predictions from the petrogenetic net (Fig.9). All calculations were done using method 1 (Table 2) with multivariant reactions listed in Table 3 (E10-20). In the biotite zone, the temperature can be approximated calculating reaction E10 (curve 3a in Fig.9) and the minimum pressure with reaction E11 (curve 3b in Fig.9) involving a theoretical K-feldspar. For mica-schist 01CH29 approximate conditions at 2-3 kbar, 400-450°C result. PT-conditions in the medium grade rocks can be estimated in two ways: (1) Overstepping the staurolite in-reaction conditions in the andalusite stability field are ~520-580°C, 2.5-3 kbar around the isopleth $X_{Fe}=0.9$ for garnet coexisting with staurolite, biotite, muscovite and quartz (Spear & Cheney 1989; curve 4 in Fig.9). (2) Invariant point 5 in Fig.9 was calculated on the basis of the three water-independent reactions E12-E14. For sample 01CH42 conditions of 555°C, 3.2 kbar result.

Evaluation of the highest grade conditions are as follows: (1) Fe-Mg-exchange thermometry for cordierite-biotite pairs (Bhattacharya et al. 1988) in sample 01CH48 results at 684-716°C (point 8 in Fig.9) and the isopleth $X_{Fe}=0.85$ for garnet coexisting with cordierite, biotite, K-feldspar and quartz occurs at 650°C (curve 7 in Fig.9). The position of the univariant reaction $Bt + Sil + Qtz = Grt + Cord + Kfs + H_2O$ in this temperature range indicates a minimum of 2.5-3.2 kbar. (2) An invariant point (point 6 in Fig.9) was calculated intersecting 7 multivariant water-independent reactions (E15-E20, E12) including coexisting cordierite, biotite, garnet, quartz, sillimanite and plagioclase. For sample 01CH48 peak conditions at 690°C, 3.45 kbar result. Using water-dependent multivariant reactions including the same components as well as K-feldspar (9 reactions) a reduced water activity can be estimated at ~0.5.

Intrusion depth of the neighbouring granite (98CH43) was approximated using the zoned magmatic muscovite coexisting with biotite and K-feldspar. Intersection of reaction E11 with the wet granite solidus is at 3.6 kbar for an Si-content of 3.08 apfu in white mica cores (curve 9a in Fig.9) and at 2.8 kbar for Si 3.04 apfu in the white mica rims (curve 9b). The quartz-muscovite breakdown curve is considerably lowered for Si 3.08 apfu (curve 2b in Fig.9). Hence most muscovite presumably crystallized near the granite solidus just on the low temperature side of the muscovite+quartz-breakdown curve.

7. DISCUSSION AND GEODYNAMIC CONSTRAINTS

The petrological information from the paired metamorphic belt derived in this study can contribute to a tentative reconstruction of the approximate thermal structure of the former continental margin and its geometric constraints. The resulting conceptual model is presented in Fig. 10.

7.1 The evolution of the accretionary prism

The protoliths of the metabasites and metapsammopelites in the Western Series are of very different origin, i.e. from the uppermost part of the subducting oceanic plate and predominantly from the overriding continental plate (terrigenous trench filling) respectively. Nevertheless, it could be shown that their metamorphic evolution, their deformational history and their metamorphic ages (see Willner et al., this volume) is similar, which indicates a joint evolution from the earliest detectable stage. Mixture could have occurred during subduction and early basal accretion. Analogue modeling of Gutscher et al. (1998) demonstrated that effective subduction of long thick sheets of sediments is

possible with high basal friction during low angle subduction involving steep erosional frontal slopes. As shown above, the oceanic crust incorporated into the Western Series partly involved alkali basalts. This would have contributed to lighter oceanic crust leading to a decrease of the subduction angle and an uneven surface of the subducting slab due to the presence of oceanic islands.

Peak PT-conditions of the greenschist (7.0-9.3 kbar, 380-420°C) indicate metamorphism under a metamorphic gradient of 11-16°C/km (on the basis of an average density of 2.8 g/cm³), which appears relatively high for a subduction environment. However, this gradient seems to be typical for the Western Series as it was also detected in south-central and southern Chile (Willner et al. 2000, 2001). The elevated metamorphic gradient may be due to several factors: Numerical modeling by Peacock (1996) predicts that (1) slow subduction and (2) a relatively flat subducting slab may enhance the thermal gradient. (3) The subduction of upper crustal material (greywackes) with high content of radiogenic elements also contributes to the heat production at depth. A further factor (4) is envisaged here: Analogue modeling has recently shown that basal accretion during flat subduction may involve formation of long flat duplexes forming an antiformal stack (Kukowski et al. 2002). This is tentatively included in the conceptual model (Fig.10). Such process predicts that part of the accreted material will initially move horizontally away from the lower plate before vertical exhumation and thus cross isotherms towards higher temperature at maximum depth. A near-isobaric late prograde PT-path (particle path 1 in Fig.10) can be expected, although it could not be deduced for the studied rocks. However, a late prograde heating with little pressure variation is known from albite amphibolite grade rocks of comparable settings (Chonos Archipelago/Chile: Willner et al. 2000; South Shetland Islands: Trouw et al. 1998). Pervasive subhorizontal foliation (s_2 , locally s_3) mainly originated during peak PT-conditions. It reflects basal accretion and crustal thinning at depth following basal accretion. The occurrence of glaucophane-bearing blueschist must be considered as extremely rare, because only three localities are known along the ~1500 km of basement exposure of the Coastal Cordillera (Willner et al. 2004 a, b) implying a special preservation mode. This rock was metamorphosed to significantly different peak PT-conditions at 9.5-10.7 kbar, 350-385°C corresponding to a lower metamorphic gradient (~9-11°C/km) than in the predominant greenschist. There is no difference in peak PT-ages of both neighbouring metabasite types (Willner et al., this volume). This appears problematic, because a higher peak temperature would be expected for the blueschist compared to

the greenschist, if they were metamorphosed along a gradient parallel to the subducting slab (Fig.10). More common metabasites, which were subducted to similar depth as the blueschist in other areas of the Western Series, are metamorphosed to albite-epidote-amphibolite facies (Kato 1984; Willner et al. 2000, 2004a; Trouw et al. 1998) showing comparable metamorphic gradients as the greenschist. Here it is suggested that the blueschist derived from the lowermost part of the basal accretion zone of the accretionary wedge near the uppermost tip of the mantle wedge (Fig. 10; particle path 2) and that it conserved the original gradient along the subducting slab (see Fig.10), as is also implied by Trouw et al. (1998) and Willner et al. (2004a, b) for similar settings with blueschists. However, the blueschist was not heated during exhumation. It is suggested that it was emplaced by local low-angle thrusting at depth onto the already isobarically heated greenschist.

The second “exotic” rock type is the unusual garnet mica-schist at Punta Sirena that yielded the highest PT-conditions in the entire study area (390-440°C, 9.6-14.7 kbar), which were shown to reflect a retrograde stage after presumable isobaric cooling from still higher peak temperature (particle path 3 in Fig.10). The ages for this stage are the oldest recorded in the study area (Willner et al. this volume). A geodynamic interpretation can be provided in analogy (1) to a better constrained occurrence in south-central Chile (Willner et al. 2004b), (2) to similar findings in comparable settings worldwide (e.g. Wakayabashi 1990) and (3) to numerical modeling (Gerya et al. 2003): Siliciclastic material was subducted at the earliest stage accretion activity to the deepest level under the mantle wedge and heated in contact with a still hot mantle. Later accreted material at this site caused hydration and cooling of the earliest accreted material and the overlying mantle. After this change (also of rheological conditions in the mantle), effective exhumation of the early subducted material followed at the base of the hydrated mantle wedge within a cooler environment than during its burial. The exotic garnet mica-schist thus provides important relics and time markers for the onset of subduction mass flow in the Coastal Cordillera accretionary prism. It must be noted that its predominant retrograde equilibration occurred under the same metamorphic gradient as the blueschist presumably in a position near the subducting slab (Fig.10).

In all rock types of the Western Series a similar type of partial exhumation paths involving slight cooling with decompression is preserved that is also similar to those of other HP/LT belts worldwide (e.g. Vidal & Parra 2000 and references therein). It involves decompression with only slight cooling

after peak metamorphic conditions recorded by the formation of retrograde local equilibria in the presence of free water and crystallization/recrystallization processes. The retrograde overprint occurred within a narrow temperature range of 300-400°C. Continuous reactions during pressure release of ~3-4 kbar caused further crystal growth at the rims as well as recrystallisation recording a clockwise decompression path. Further reaction to below 300°C is probably hampered for kinetic reasons. The geometry of the retrograde PT-path implies a kink after cooling through 350°C at ~4 kbar to cooling below 300°C at ~2-3 kbar (Fig.8). Late exhumation thus occurred under a high geothermal gradient implying a “doming” of isotherms above the accretionary prism (Fig.10). Retrograde mineral growth and recrystallization generally occurred under strainfree conditions. Retrograde ductile deformation is restricted to rare local shear bands indicating that there is little tectonic control of the exhumation process.

7.2 The high-temperature belt

The spatial field relationship of isograd surfaces dipping to the west and following the N-S trend of the batholith along strike indicates a close relation to a major heat input during the intrusion of the arc batholith. The HT-metamorphic overprint of regional extent in the Eastern Series involves progressively increasing temperatures from 400°C to 720°C toward the intruding batholith at a uniform shallow level at ~10 km depth (3 ± 0.5 kbar), which is also consistent with the intrusion depth of the batholith. It can be shown that the HT-metamorphism and the main intrusion pulse of the batholith is contemporaneous at ~300 Ma (Willner et al., this volume). The observed HT-metamorphism involves a nearly isobaric temperature increase, which requires a short-time massive heat input related to voluminous magma production. For the retrograde path, a short-term isobaric cooling is considered at nearly the same level to temperatures also prevailing in the neighbouring Western Series. A lack of inverse zonation in high temperature garnets precludes a long time of cooling. Contrasting the Western Series, local retrograde overprint is of very low temperature type and unrelated to the early exhumation path. Although no definite metamorphic relics prior to the HT-overprint of the Eastern Series were detected in the study area, deformation structures were overprinted that occur at very low grade conditions in the Eastern Series of other areas in the Coastal Cordillera basement (Hervé 1988).

The garnet mica-schist in the Western Series could have reached its maximum depth during subduction roughly below the magmatic arc. As will be shown by Willner et al. (this volume), its peak of metamorphism is older than the main pulse of intrusion in the magmatic arc. Considering the above inferred genetic model for the garnet mica-schist, it seems conceivable that a certain amount of siliciclastic material was subducted to great depth at an early stage giving rise to a pulse of hydrous fluids released by dehydration that could be responsible for generating the substantial amounts of magmas of the Late Paleozoic.

7.3 The conceptual model

Above considerations point to a convergent subduction regime above a relatively low angle subducting slab. Data from the study area can help to construct a conceptual model for the Lower Paleozoic convergent margin at an approximate scale (Fig.10). According to the recorded maximum PT-data and their link to the penetrative deformation, basal accretion occurred in the Western Series at a depth of ~25-40 km, while small quantities of subducted material (garnet mica-schist) reached maximum depths of ~45-50 km at an early stage. If above discussed relationship between this deeply subducted material and the main pulse of magma formation in the arc is correct, it implies a depth of ~45-50 km of the subducting slab just below the magmatic arc. The distance between the axis of the magmatic arc and the boundary of the Western and Eastern Series in the southern study area is ~30 km. This boundary marks the transition between two environments of contrasting crustal thickness and exhumation rates (Willner et al., this volume). It is assumed here that the thickness of the accretionary prism is maximum (~40 km) at this boundary. The distance of ~30 km hence marks the horizontal distance between the slab at ~40 km and at ~50 km. A dip angle of the subducting slab of ~25° and a width of the Western Series of ~40 km results. Isotherms along the subducting slab were drawn according to the metamorphic gradient indicated by the blueschist and garnet mica-schist, but at lower crustal levels according to the retrograde path of all rock types and the metamorphic zonation in the Eastern Series.

The boundary between both metamorphic units lacks an apparent shear zone juxtaposing different crustal levels and excising intermediate levels as is common in orogens worldwide. The transitional nature has been observed at several sites in the Coastal Cordillera (see Hervé 1988). The special situation can only be explained by the cyclic nature of particle paths in the accretionary prism

(Western Series), when continuous basal accretion at depth is mainly outbalanced by erosion of a forearc high at the surface as is also inferred by modeling (e.g. Kukowski et al. 2002). This creates a stack of crustal slices from the base to the top of the crust with a similar metamorphic and deformational imprint. The retrowedge (Eastern Series) including the magmatic arc remained relatively stationary in its position during accretion. Brittle thrusting of the Eastern Series on top of the Western Series as observed in the north of the study area occurred in an upper crustal level a long time after accretion had ceased (Willner et al., this volume). This is rather related to a late shortening of the convergent margin.

The oceanward continuation of the Western Series, i.e. the part of the prism with frontal accretion, is nowhere observed in the Coastal Cordillera basement. However, within the offshore continuation of continental crust of ~50-80 km toward the west relics of this missing frontal accretion zone might still be preserved. Hence in the study area a nearly intact Late Paleozoic convergent margin including an accretionary prism and a magmatic arc is preserved, where continuous basal accretion of mainly siliciclastic material and minor uppermost oceanic crust occurred over a limited range of time and above a low angle subducting slab.

ACKNOWLEDGEMENTS

This research was financially supported by a grant of Deutsche Forschungsgemeinschaft (Wi875/8-1,2) and the German-Chilean BMBF-CONICYT cooperation project ChI 01A 6A "High pressure metamorphic rocks in Chile". E.Godoy and F.Hervé (both Santiago) are particularly thanked for many discussions and multiple support over years. The paper was considerably improved by the careful review of O.Vidal. H.-J.Bernhardt (Bochum) provided microprobe facilities for considerable time. This study is a contribution to IGCP 436 "Pacific Gondwana Margin".

REFERENCES

- Aguirre, L., Hervé, F. & Godoy, E. (1972). Distribution of metamorphic facies in Chile: an outline. *Krystallinikum* **9**, 7-19.
- Bhattacharya, A., Mazumdar, A.C. & Sen, S.K. (1988). Fe-Mg mixing in cordierite: constraints from natural data and implications for cordierite-garnet geothermometry in granulites. *Am. Mineral.* **73**, 338-344.
- Berman, R.G. (1988). Internally-consistent thermodynamic data for minerals in the system Na₂O-K₂O-CaO-MgO-FeO-Fe₂O₃-Al₂O₃-SiO₂-TiO₂-H₂O-CO₂. *J. Petrol.* **29**, 445-522.
- Berman, R.G. (1990). Mixing properties of Ca-Mg-Fe-Mn garnets. *Am. Mineral.* **75**: 328-344.
- Brown, T.H., Berman, R.G. & Perkins, E.H. (1989). Ge0-Calc: Software package for calculation and display of pressure-temperature-composition phase diagrams using an IBM or compatible Personal Computer. *Computer & Geoscience* **14**, 279-289.
- Bravo Espinosa, P.J. (2001). Geología del borde oriental de la cordillera de la costa entre los ríos Mataquito y Maule, VII región. B.Sc. thesis, Universidad de Chile, Santiago, 113 p. (unpublished).
- Dale J., Holland, T.J.B. & Powell, R. (2000). Hornblende-garnet-plagioclase thermobarometry: a natural assemblage calibration of the thermodynamics of hornblende. *Contrib. Mineral. Petrol.* **140**, 353-362
- De Capitani, C. & Brown, T.H. (1987). The computation of chemical equilibrium in complex systems containing non-ideal solid-solutions. *Geochim. Cosmochim. Acta* **51**, 2639-2652.
- Evans, B.W. (1990). Phase relations of epidote-blueschists. *Lithos* **25**, 3-23.
- Gana, P. & Hervé, F. (1983). Geología del basamento cristalino en la Cordillera de la Costa entre los ríos Mataquito y Maule, VII region. *Rev.Geol.Chile* **19-20**, 37-56.
- Gerya, T.V., Maresch, W.V., Willner, A.P., Van Reenen, D.D. & Smit, C.A. (2001). Inherent gravitational instability of thickened continental crust with regionally developed low- to medium-pressure granulite facies metamorphism. *Earth Planet. Sci. Lett.* **190**, 221-235.
- Gerya, T.V., Stöckhert, B. & Perchuk, A.L. (2003). Exhumation of high-pressure metamorphic rocks in a subduction channel – a numerical simulation. *Tectonics* **142**, 6-1 - 6-19.

- Godoy, E. (1970). Estudio petrográfico del granito de Constitución y su aureola de metamorfismo de contacto. Unpubl. B.Sc. thesis Univ. Chile Santiago, 130 p.
- Godoy, E. (1986). Die Entwicklung des Gondwana-Randes in Chile während des Paläozoikums unter besonderer Berücksichtigung der geotektonischen Stellung der Metavulkanite. Doct. thesis Univ. Münster/Germany, 70 p. (unpublished).
- Godoy, E. & Kato, T. (1990). Late Paleozoic serpentinites and mafic schists from the Coast Range accretionary complex, Central Chile: their relation to aeromagnetic anomalies.- *Geol. Rdschau* **79**, 121-130.
- González Bonorino, F. (1971). Metamorphism of the crystalline basement of central Chile. *J. Petrol.* **12**, 149-175.
- Gutscher, M.A., Kukowski, N., Malavieille, J. & Lallemand, S. (1998). Material transfer in accretionary wedges from analysis of a systematic series of analog experiments. *J. Struct. Geol.* **20**, 407-416.
- Hervé, 1988. Late Paleozoic subduction and accretion in Southern Chile. *Episodes* **11**, 183-188.
- Holland, T.J.B. (1980). The reaction albite = jadeite + quartz determined experimentally in the range 600-1200°C. *Amer. Mineral.* **65**, 129-134.
- Holland, T.J.B. & Powell, R. (1998a). An internally consistent thermodynamic data set for phases of petrological interest. *J. metam. Geol.* **16**, 309-343.
- Holland, T.J.B. & Powell, R. (1998b). Mixing properties and activity-composition relationships of chlorites in the system MgO-FeO-Al₂O₃-SiO₂-H₂O. *Eur. J. Min.* **10**, 395-406.
- Johannes, W. (1984). Beginning of melting in the granite system Qz-Or-Ab-An-H₂O. *Contrib. Mineral. Petrol.* **86**, 264-273.
- Kato, T.T. (1985). Pre-Andean orogenesis in the Coast Ranges of Central Chile. *Geol. Soc. Am. Bull.* **96**, 918-924.
- Kretz, R. (1983). Symbols for rock-forming minerals. *Am. Mineral.* **68**, 277-279.
- Kukowski, N., Lallemand, S.E., Malavieille, J., Gutscher, M.A. & Reston, T.J. (2002). Mechanical decoupling and basal duplex formation observed in sandbox experiments with application to the Western Mediterranean Ridge accretionary complex. *Marine Geology* **186**, 29-42.

- Leake, B.E. and 21 others (1997). Nomenclature of amphiboles. Report of the subcommittee on amphiboles of International Mineralogical Association Committee on New Minerals and Mineral Names. *Eur. J. Mineral.* **9**, 623-651.
- Leterrier, J., Maury, R., Thonon, P., Girard, D. & Marchal, M. (1982). Clinopyroxene composition as a method of identification of magmatic affinities of paleovolcanic series. *Earth Planet Sci. Lett.* **59**, 139-154.
- Lucassen, F., Trumbull, R., Franz, G., Creixell, C., Vásquez, P., Romer, R.L. & Figueroa, O. (2004): Distinguishing crustal recycling and juvenile additions at active continental margins: the Paleozoic to recent compositional evolution of the Chilean Continental margin (36°-41S). *J. S. Amer. Earth Sci.* (in press).
- McMullin, D.W., Berman, R.G. & Greenwood, H.J. (1991). Calibration of the SGAM thermometer for pelitic rocks using data from equilibrium experiments and natural assemblages. *Can. Mineral.* **29**, 889-908.
- Martin, M.W., Kato, T.T., Rodriguez, C., Godoy, E., Duhart, P., McDonough, M. & Campos, A. (1999). Evolution of the late Paleozoic accretionary complex and overlying forearc-magmatic arc, south central Chile (38°-41°S): Constraints for the tectonic setting along the southwestern margin of Gondwana. *Tectonics* **18**, 582-605.
- Massonne, H.-J. & Schreyer, W. (1986). High-pressure syntheses and X-ray properties of white micas in the system K_2O - MgO - Al_2O_3 - SiO_2 - H_2O .- N. Jb. Miner. Abh. **153**, 177-215.
- Massonne, H.-J. (1995a). P-T evolution of metavolcanics from the southern Taunus mountains. In Dallmeyer, R.D., Franke, W., Weber, K. (Eds.): *Pre-Permian geology of Central and Eastern Europe*. 132-137, Berlin-Heidelberg (Springer).
- Massonne, H.-J. (1995b). Experimental and petrogenetic study of UHPM. In: Coleman, R.G., Wang, X. (Eds.): *Ultrahigh pressure metamorphism*. 33-95, Cambridge (Cambridge University Press).
- Massonne, H.-J. (1997). An improved thermodynamic solid solution model for natural white micas and its application to the geothermobarometry of metamorphic rocks. *Geol. Surv. Finland, Guide 46, Mineral equilibria and databases, Abstracts*, 49.

- Massonne, H.-J. & Szpurka, Z. (1997). Thermodynamic properties of white micas on the basis of high-pressure experiments in the systems K_2O - MgO - Al_2O_3 - SiO_2 - H_2O and K_2O - FeO - Al_2O_3 - SiO_2 - H_2O . *Lithos* **41**, 229-250.
- Moraga, J. (1981). Geología de la Cordillera de la Costa entre Punta Sirena y el Rio mataquito. Unpubl. B.Sc. thesis Univ.Chile Santiago
- Nisbet, E.G. & Pearce, J.A. (1977). Clinopyroxene composition in mafic lavas from different tectonic settings. *Contrib. Mineral. Petrol.* **63**, 149-160.
- Parra, T., Vidal, O. & Jolivet, L. (2002a). Relation between the intensity of deformation and retrogression in blueschist metapelites of Tinos Island (Greece) evidenced by chlorite-mica local equilibria. *Lithos* **63**, 41-66.
- Parra, T., Vidal, O., Agard, P. (2002b). A thermodynamic model for Fe-Mg dioctahedral K-white micas using data from phase equilibrium experiments and natural pelitic assemblages. *Contrib.Mineral. Petrol.* **143**, 706-732.
- Peacock, S.M. (1996). Thermal and petrologic structure of subduction zones. In Behout, G.E., Scholl, D.W., Kirby, S.H., Platt, J. (eds.): *Subduction - top to bottom. Am Geophys Union, Geophys Monograph* **96**, 119-131
- Powell, R., Holland, T.J.B. (1999). Relating formulations of the thermodynamics of mineral solid solutions: activity modeling of pyroxenes, amphiboles and micas. *Am. Mineral.* **84**, 1-14.
- Spear, F.S & Cheney, JT (1989). A petrogenetic grid for pelitic schists in the system SiO_2 - Al_2O_3 - FeO - MgO - K_2O - H_2O . *Contrib. Mineral. Petrol.* **101**, 149-164.
- Trouw, R.A.J., Simoes, L.S.A. & Valladares, C.S. (1998). Metamorphic evolution of a subduction complex, South Shetland Islands, Antarctica. *J. Metamorph. Geol.* **16**: 475-490.
- Vidal, O. & Parra, T. (2000). Exhumation paths of high-pressure metapelites obtained from local equilibria for chlorite-phengite assemblages. *Geol. J.* **35**, 139-161.
- Vidal, O., Parra, T. & Trotet, F. (2001). A thermodynamic model for Fe-Mg aluminous chlorite using data from phase equilibrium experiments and natural pelitic assemblages in the 100-600°C, 1-25 kbar range. *Am. J. Sci.* **6**, 557-592.

- Vinograd, V.L. (2002a). Thermodynamics of mixing and ordering in the diopside-jadeite system: I. A CVM model. *Min. Mag.* **66**, 513 – 536.
- Vinograd, V.L. (2002b). Thermodynamics of mixing and ordering in the diopside-jadeite system: II. A polynomial fit to the CVM results. *Min. Mag.* **66**, 537 – 545.
- Wakabayashi, J. (1990). Counterclockwise PTt paths from amphibolites, Franciscan Complex, California: relics from the early stages of subduction zone metamorphism. *J. Geol.* **98**, 657-680.
- Will, T., Okrusch, M., Schmädicke, E., Chen, G. (1998). Phase relations in the greenschist-blueschist-amphibolite-eclogite facies in the system Na₂O-CaO-FeO-MgO-Al₂O₃-SiO₂-H₂O (NCFMASH), with application to metamorphic rocks from Samos, Greece. *Contrib Mineral Petrol* **132**, 85-102.
- Willner, A.P., Hervé, F. & Massonne, H.-J. (2000). Mineral chemistry and pressure-temperature evolution of two contrasting high-pressure-low-temperature belts in the Chonos Archipelago, Southern Chile. *J. Petrol.* **41**, 309-330.
- Willner, A.P., Pawlig, S., Massonne, H.-J. & Hervé, F. (2001). Metamorphic evolution of spessartine quartzites (coticules) in the high pressure/low temperature complex at Bahia Mansa (Coastal Cordillera of Southern Central Chile). *Can. Mineral.* **39**, 1547-1569.
- Willner, A.P., Hervé, F., Thomson, S.N. & Massonne, H.-J. (2004a). Converging P-T paths of Mesozoic HP-HT metamorphic units (Diego de Almagro Island, Southern Chile): evidence for juxtaposition during late shortening of an active continental margin. *Mineral. Petrol.* **81**, 43-84
- Willner, A.P., Glodny, J., Gerya, T.V., Godoy, E. & Massonne, H.-J. (2004b) A counterclockwise PTt-path of high pressure-low temperature rocks from the Coastal Cordillera accretionary complex of south-central Chile: constraints for the earliest stage of subduction mass flow. *Lithos* **75**, 283-310.
- Willner, A.P., Thomson, S.N., Kröner, A., Wartho, J.A., Wijbrans, J.R. & Hervé, F. Time markers for the evolution and exhumation history of an Upper Paleozoic paired metamorphic belt in Central Chile (34°-35°30'S). *J. Petrol.* (this volume)

Figure Captions

Fig.1 Geological map of the paired metamorphic belt within the basement of the Coastal Cordillera in north-central Chile (34° and 35°30'S) and its cover rocks. Information is included from Godoy (1970),

Gonzalez Bonorino (1971), Moraga (1981), Gana & Hervé (1983), Bravo Espinosa (2001) and own observations.

Fig.2 MnO-TiO₂-Na₂O variation diagram for magmatic clinopyroxene in metabasite and its compositional range in reference rock types (Nisbet & Pearce 1977).

Fig.3 Variation diagrams of amphibole in blueschist (a-c; including ferruginous metasediment 98CH25) and greenschist (d,e). c,e – Variation of end members: $X_{\text{Glauc}} = (2-\text{Ca})/2 * {}^{\text{VI}}\text{Al} / ({}^{\text{VI}}\text{Al} + \text{Fe}^{3+})$; $X_{\text{Act}} = \text{Ca}/2$; $X_{\text{Rieb}} = 1 - (X_{\text{Rieb}} + X_{\text{Act}})$ with solvus as calculated by Massonne (1995a).

Fig.4. Maps of X-ray intensity distribution for Ca, Na and Mg in a zoned glaucophane (core) overgrown by a Na-Ca-amphibole rim (blueschist sample 95CH11). Relative intensities increase from light to dark gray.

Fig.5 Si-Al variation diagram of white mica within all studied rock types.

Fig.6 P-T pseudosections calculated for representative whole rock compositions of metabasite and metapsammopelite samples in the system: SiO₂ - TiO₂ - Al₂O₃ - Fe₂O₃ - FeO - MgO - CaO - Na₂O - K₂O - H₂O. For thermodynamic data and activity models see Table 2. Abbreviations not following Kretz (1983) are: Kwm – K-white mica; Nam – Na-amphibole; Cam –Ca-amphibole; V - vapour. Analyses were done at Ruhr-Universität Bochum by XRF except Fe²⁺ and H₂O (standard wet chemical methods).

Fig.7 P-T maps showing isolines of calculated ratios $X_{\text{free H}_2\text{O}} / X_{\text{total H}_2\text{O}}$ in assemblages calculated from whole rock analyses (see pseudosections in Fig.6).

Fig.8 PT-estimates and partial PT-paths for rocks of the Western Series (blueschist, greenschist, metapsammopelite, garnet mica-schist); reactions calculated with average compositions (method 1; Table 2): A – stilpnomelane+phengite breakdown; B – pumpellyite + chlorite breakdown; C - garnet-amphibole thermometry (Fe-metasediments); calculation of reactions and invariant points for blueschist and greenschist with method 1, for metapsammopelite and garnet mica-schist with method 2 (Table2); upper stability of albite after Holland (1980).

Fig.9 Petrogenetic grid for rocks of the Eastern Series. The approximate PT-variation is indicated by the grey bar. Unnumbered curves are from Spear & Cheney (1989). 1 - Johannes (1984); 2a - calculated for pure phases, 2b - calculated for muscovite with Si 3.06 apfu; 3a – reaction E10 and 3b

– reaction E11 (Table 3) calculated for compositions in sample 01CH29; 4 - $X_{\text{Fe}}=0.9$ in garnet coexisting with staurolite, biotite, quartz and muscovite (Spear & Cheney 1989); 5 - calculated invariant point (reactions E12-E14 in Table 3) for the assemblage garnet-muscovite-biotite-quartz in sample 01CH43; 6 - calculated invariant point (reactions E12, E15-E20; Table 3) for the assemblage garnet-cordierite-biotite-sillimanite-plagioclase-K-feldspar-quartz in sample 01CH48; 7 – $X_{\text{Fe}} = 0.85$ in garnet in assemblage with cordierite, biotite, quartz and K-feldspar (Spear & Cheney 1989); 8 - Fe-Mg exchange thermometer for garnet-cordierite in sample 01CH43; 9a – calculated Si 3.08 apfu-, 9b - Si 3.04 apfu-isopleth for muscovite coexisting with biotite, K-feldspar and quartz (reaction E11 in Table 3). Measured mineral compositions were plotted in inset AFM-projections.

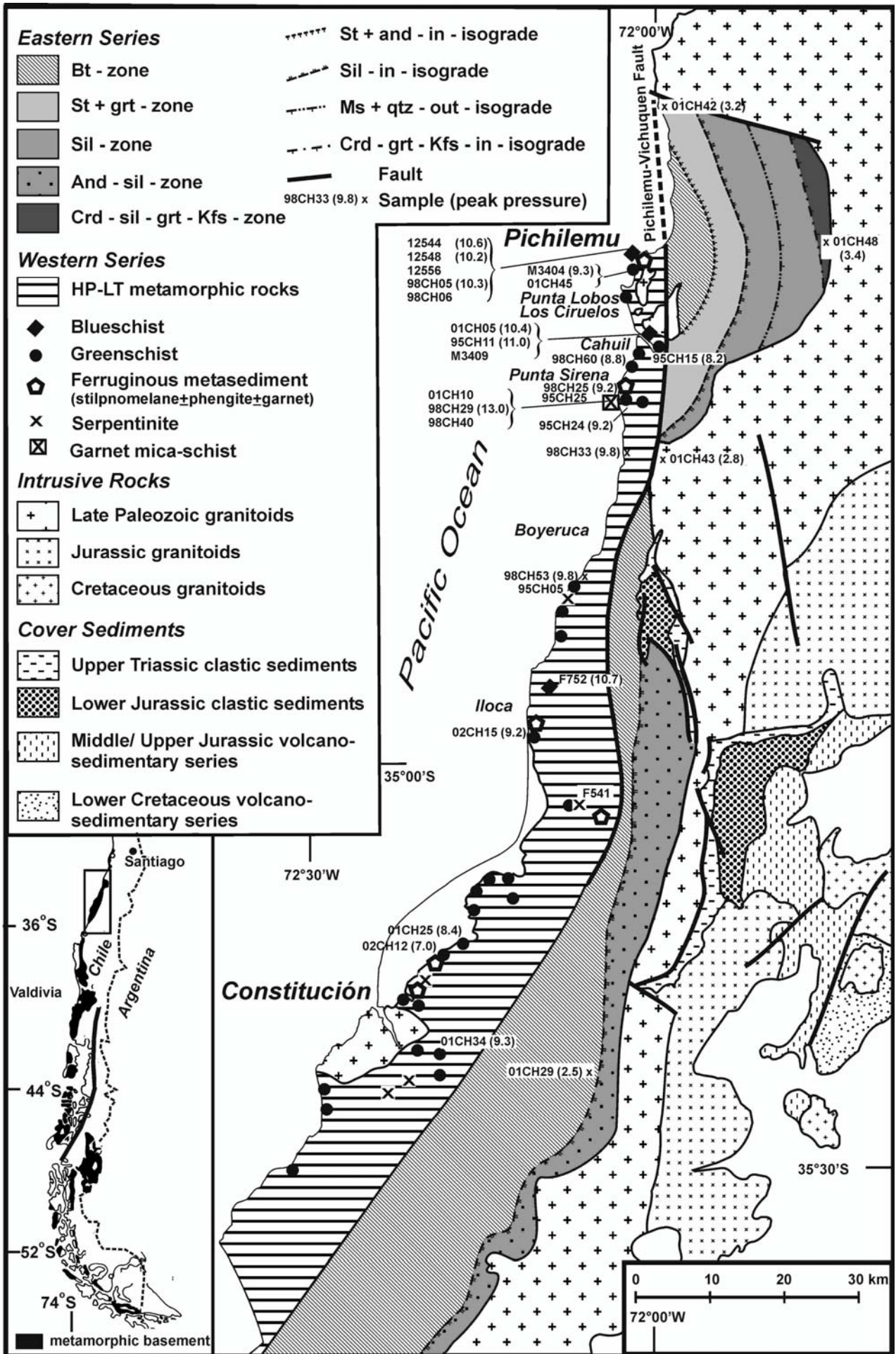
Fig.10 Conceptual model for the convergent margin of central Chile during Late Paleozoic times. Tentative depth-temperature and particle paths in the Western Series: 1-greenschist; 2-blueschist; 3-garnet mica-schist. 4-level of isobaric heating and cooling in Eastern Series.

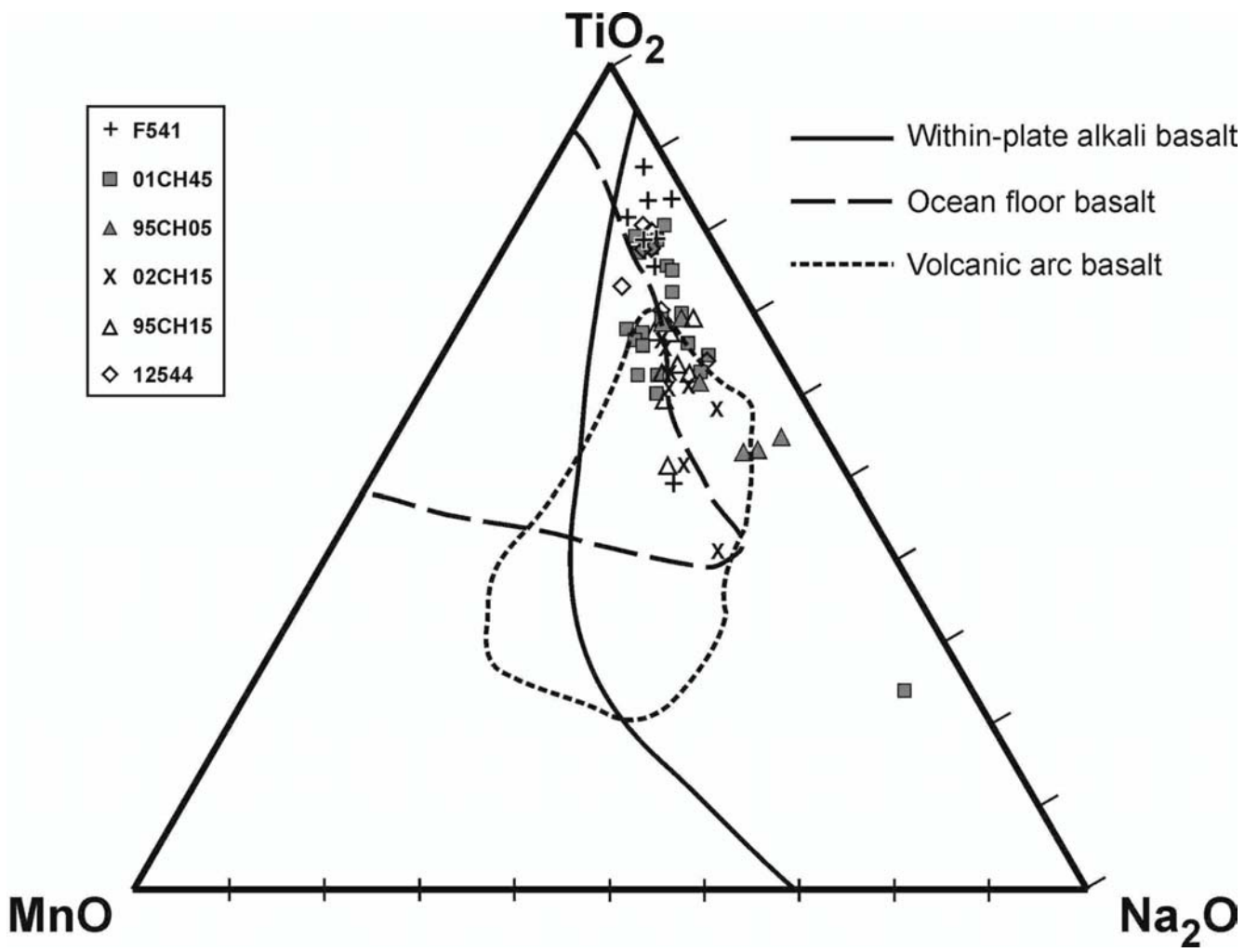
Tables

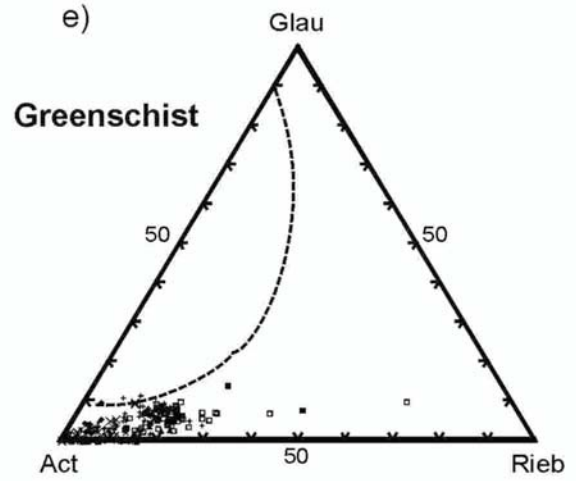
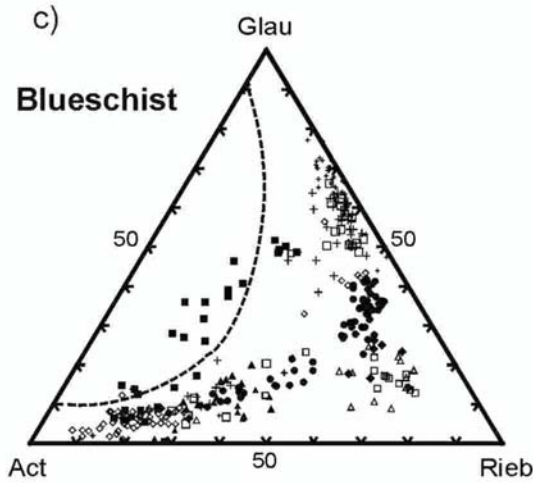
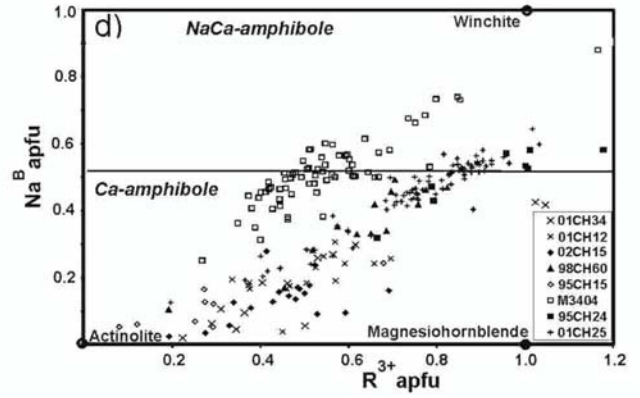
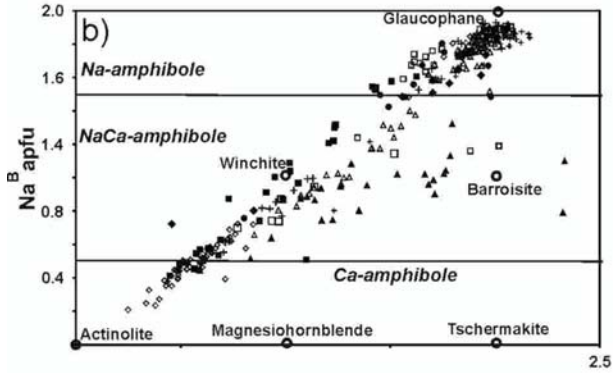
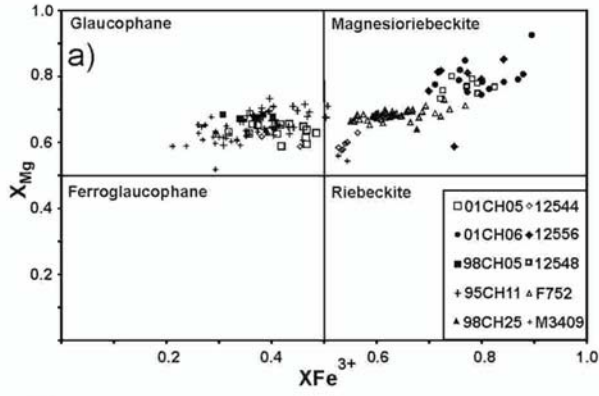
Table 1 Representative mineral analyses. An extended table including all compositions used for calculations is given in the electronic deposit of the journal.

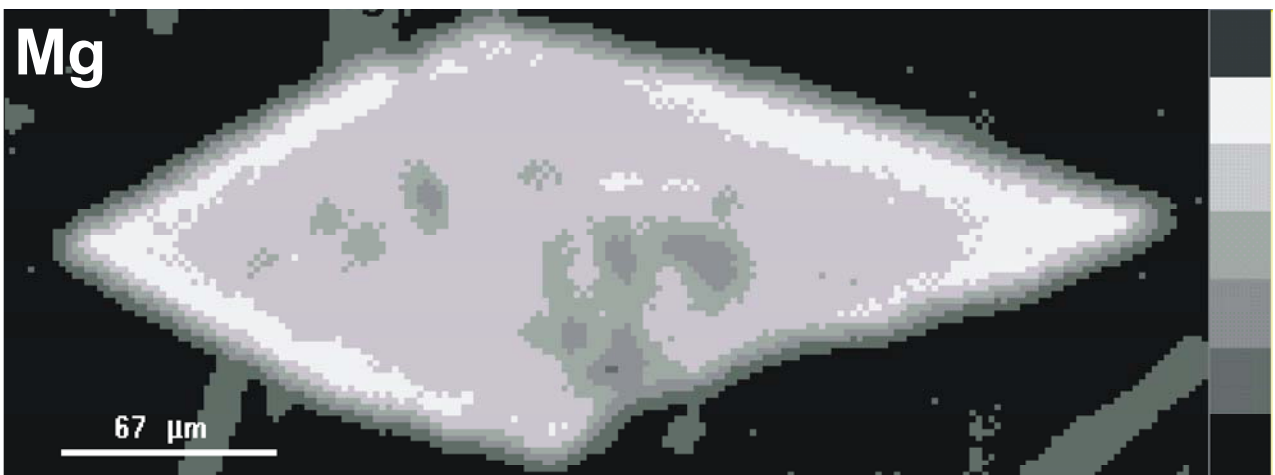
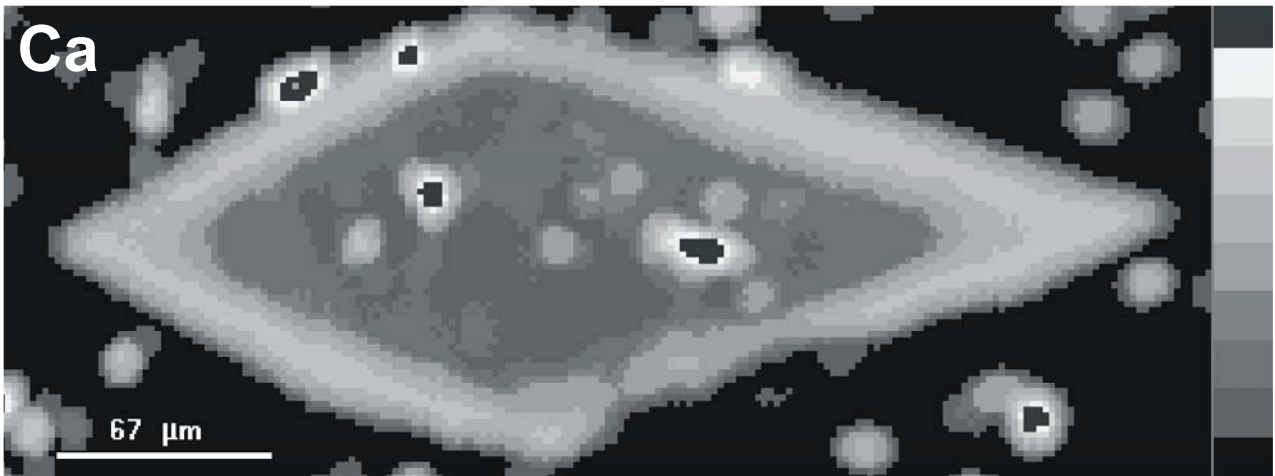
Table 2 References for thermodynamic data and activity models used for the different geothermobarometric approaches

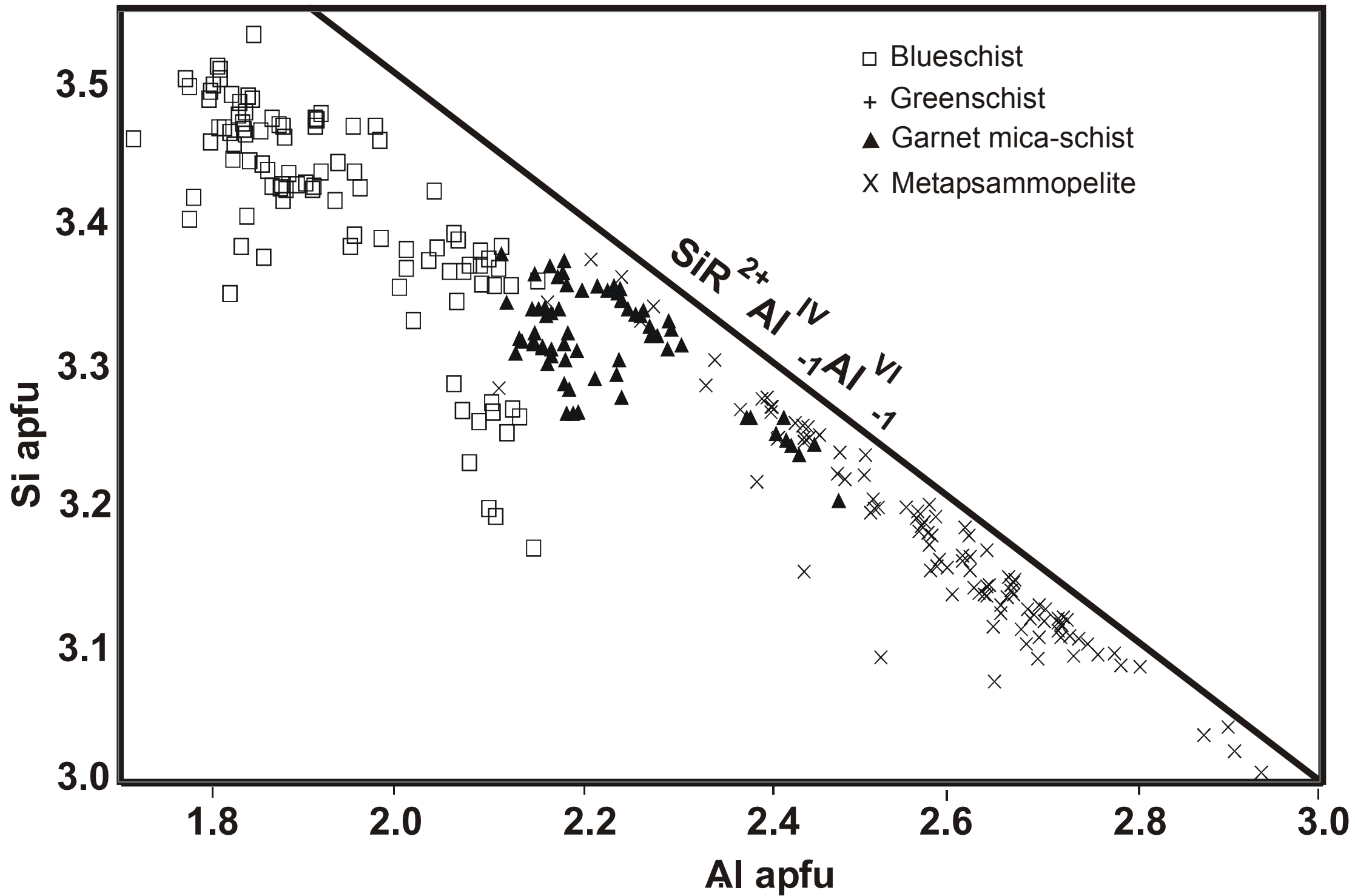
Table 3 List of calculated multivariant reactions

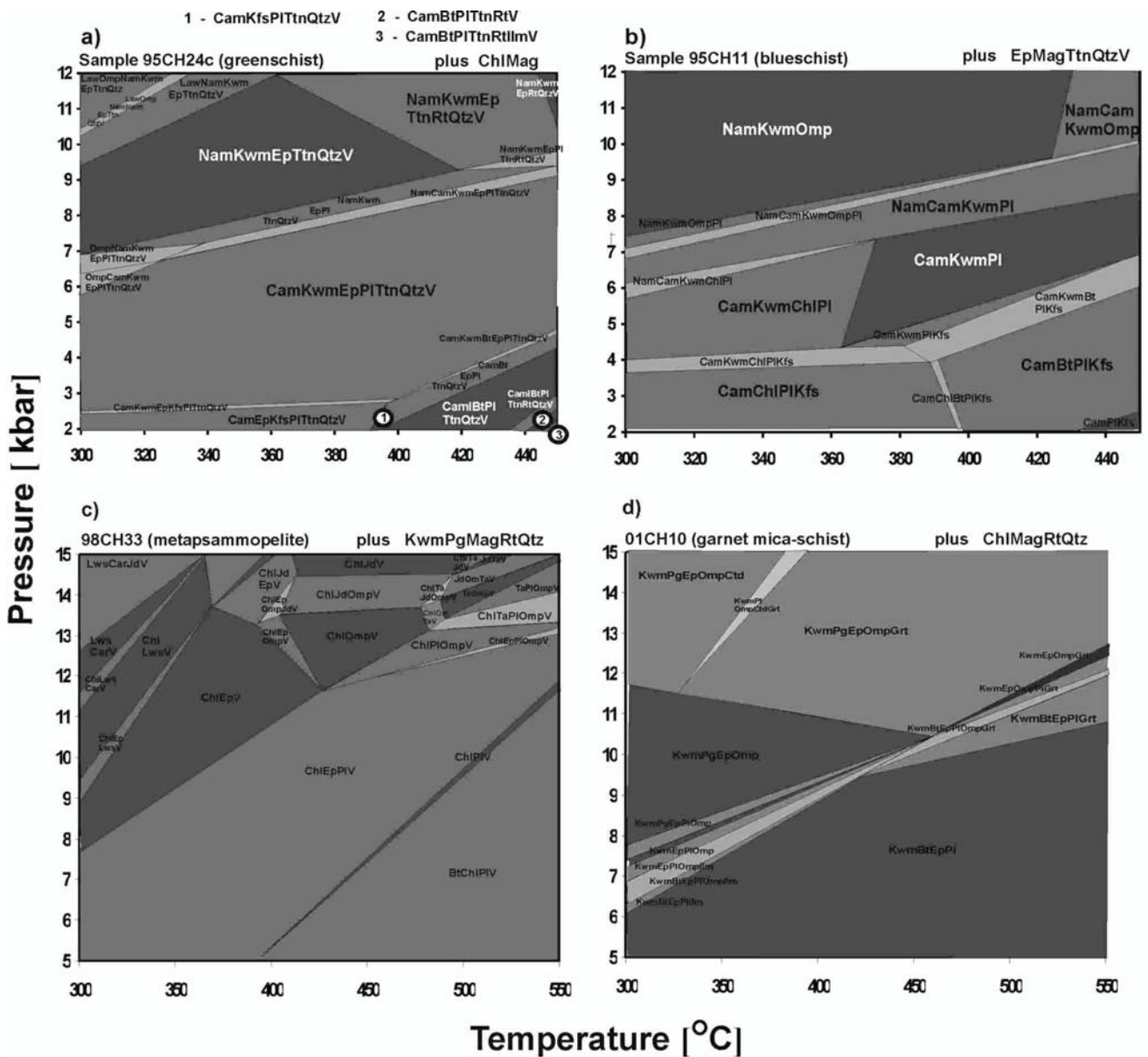






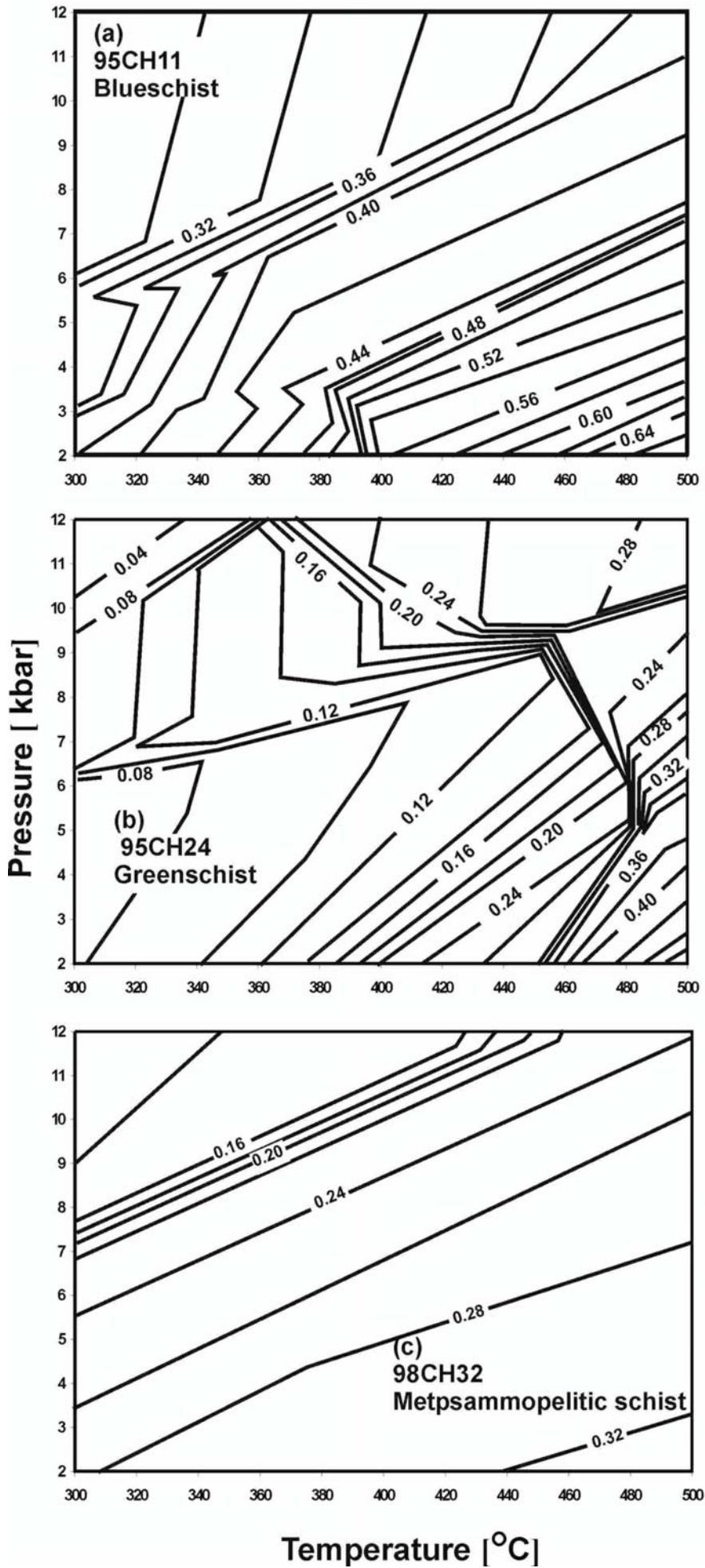


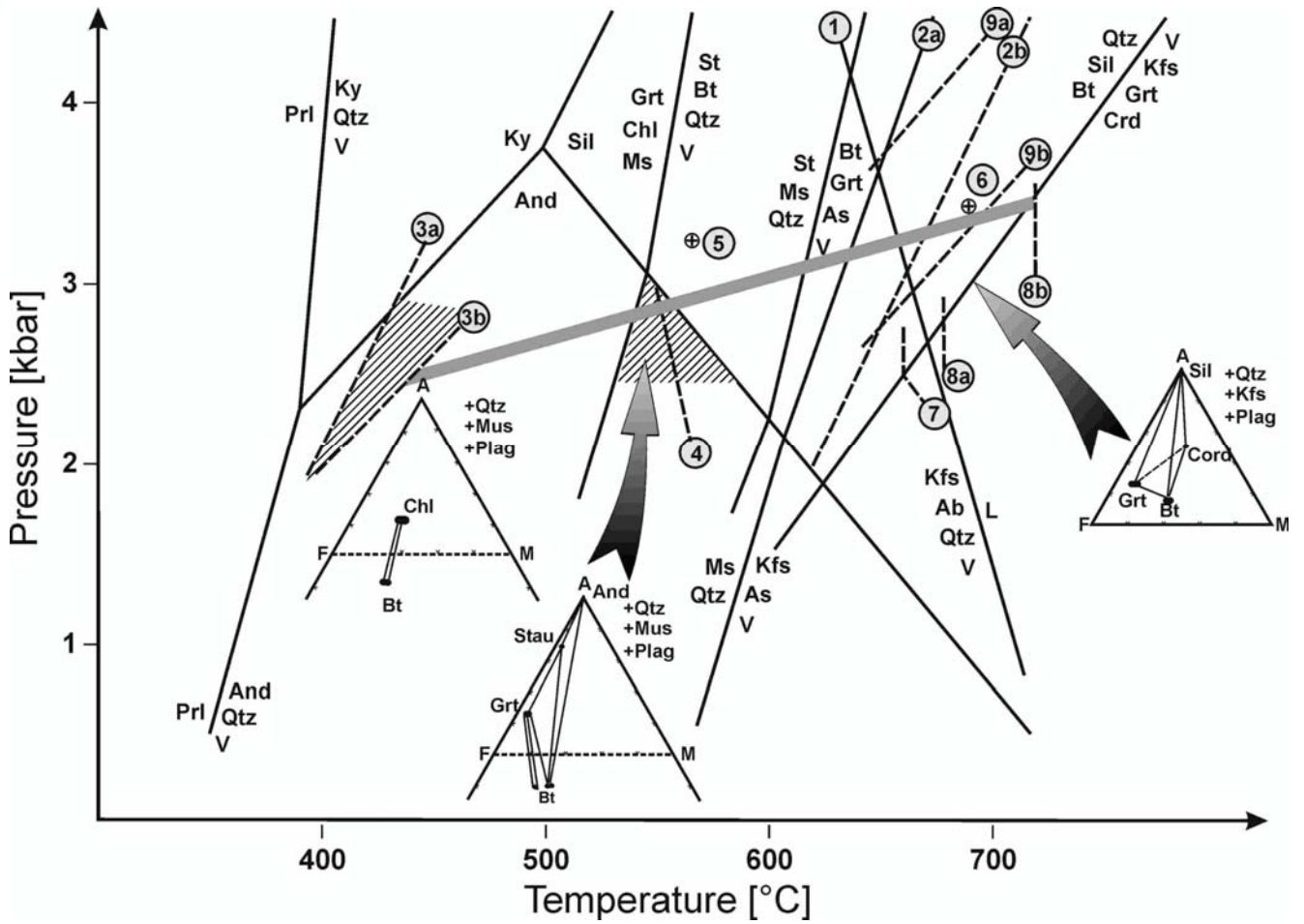
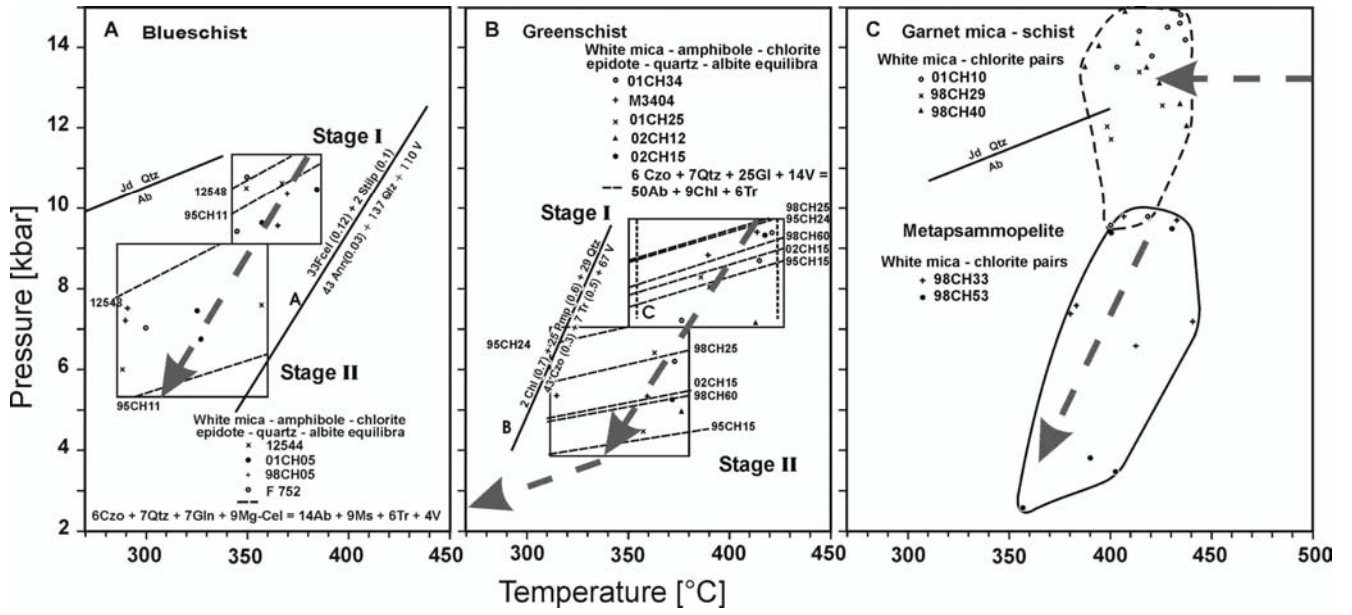




wt%	95Ch24c	95CH11	98CH33	98CH32	01CH10
SiO ₂	46.50	47.71	61.92	47.39	53.12
TiO ₂	2.53	1.89	0.87	1.22	1.04
Al ₂ O ₃	13.34	13.70	18.04	22.57	17.26
Fe ₂ O ₃	4.46	9.79	2.99	2.96	4.51
FeO	9.65	3.21	3.10	5.89	4.96
MgO	7.59	5.18	2.12	2.82	4.39
CaO	5.71	11.24	0.20	1.68	5.62
Na ₂ O	3.83	2.51	3.08	0.93	1.56
K ₂ O	0.07	1.37	3.22	5.87	2.12
H ₂ O	4.14	2.81	3.52	5.10	3.65
Sum	99.09	100.09	99.28	97.85	98.62

Divariant
 Trivariant
 Quadrivariant





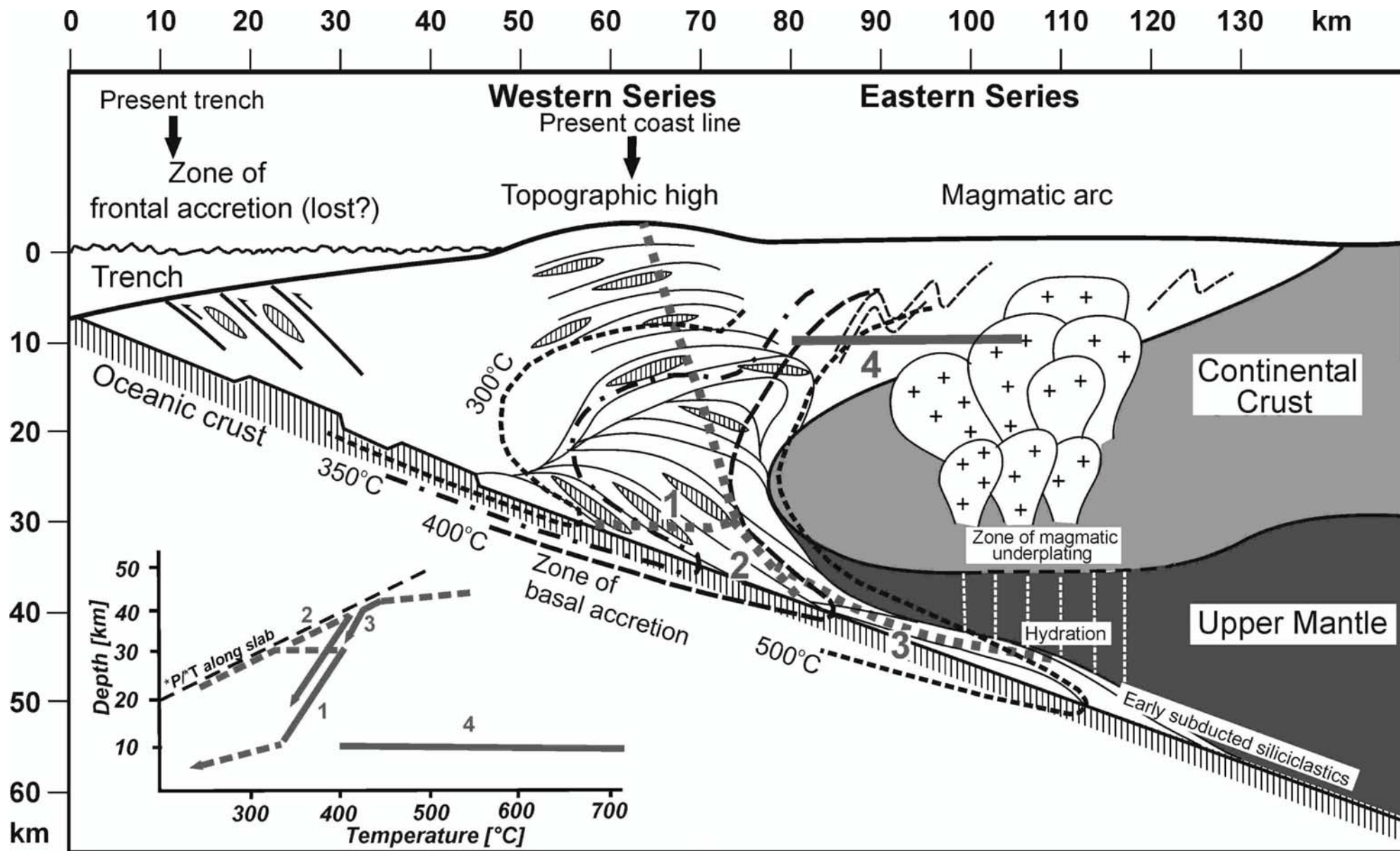


Table 1 Representative mineral analyses. An extended table including all compositions used for calculations

is given in the electronic deposit of the journal.

	Clinopyroxene			Garnet				Eastern Series			
	<i>Ultrabasite</i>	<i>Greenschist</i>	<i>Blueschist</i>	<i>Fe-Metasediment</i>		<i>Garnet mica-schist</i>		<i>Mica-schist</i>		<i>Gneiss</i>	
	<i>F541</i>	<i>01CH45</i>	<i>12544</i>	<i>98CH25C</i>	<i>98CH25R</i>	<i>01CH10C</i>	<i>01CH10R</i>	<i>98CH43C</i>	<i>98CH43R</i>	<i>01CH48C</i>	<i>01CH48R</i>
SiO ₂	49,09	50,47	50,03	35,85	35,97	36,52	37,09	36,22	35,96	36,36	36,31
TiO ₂	1,90	0,87	0,84	0,01	0,00	0,28	0,16	0,07	0,01	0,00	0,08
Al ₂ O ₃	4,89	2,75	3,58	19,02	20,14	20,91	21,47	21,01	21,07	21,26	21,18
Cr ₂ O ₃	0,78	0,08	nd	0,01	0,00	0,03	0,02	nd	nd	nd	nd
Fe ₂ O ₃ ¹⁾	1,14	3,33	2,62	2,58	1,52	0,69	0,08	0,12	0,38	0,85	1,12
FeO	4,07	4,87	4,92	12,17	14,91	21,58	26,44	31,98	39,08	35,90	36,06
MnO	0,17	0,18	0,14	23,56	18,76	10,24	2,53	8,43	1,26	1,40	1,35
MgO	14,62	14,76	15,08	0,40	0,76	0,46	1,55	1,12	1,42	3,69	3,46
CaO	22,57	22,27	21,74	6,99	7,87	9,28	10,43	1,25	1,05	0,93	1,27
Na ₂ O	0,26	0,27	0,17								
Sum	99,49	99,85	99,12	100,59	99,93	99,99	99,77	100,20	100,23	100,39	100,83
Si	1,822	1,878	1,867	5,953	5,912	5,898	5,926	5,925	5,888	5,856	5,834
Al ^{IV}	0,178	0,122	0,133	0,047	0,089	0,102	0,074	0,075	0,112	0,144	0,166
Al ^{VI}	0,036	0,000	0,025	3,675	3,812	3,879	3,969	3,976	3,952	3,891	3,846
Ti	0,053	0,024	0,024	0,001	0,000	0,034	0,020	0,009	0,001	0,000	0,010
Cr	0,023	0,002	nd	0,002	0,000	0,004	0,002	nd	nd	nd	nd
Fe ³⁺	0,032	0,093	0,073	0,323	0,188	0,083	0,009	0,015	0,047	0,109	0,144
Fe ²⁺	0,126	0,152	0,154	1,367	1,861	2,915	3,533	4,375	5,350	4,835	4,846
Mn	0,005	0,006	0,005	0,099	0,186	0,111	0,368	0,272	0,346	0,885	0,829
Mg	0,809	0,818	0,839	3,314	2,612	1,401	0,342	1,167	0,175	0,192	0,184
Ca	0,898	0,886	0,869	1,244	1,386	1,606	1,785	0,219	0,184	0,160	0,219
Na	0,019	0,020	0,012								

Normalisation to 4 cations to calculate Fe³⁺ Cations based on 48 valencies including 10 cations in the tetrahedral and octahedral sites to calculate Fe³⁺; C-core; R-rim

	Titanite			Garnet		Epidote		Blueschist		Greenschist		Ferruginous		Garnet	
	<i>Blueschist</i>	<i>Greenschist</i>	<i>Mica-schist</i>	<i>Blueschist</i>		<i>Greenschist</i>		<i>Blueschist</i>		<i>Greenschist</i>		<i>Ferruginous</i>		<i>Garnet</i>	
	<i>98Ch05</i>	<i>M3404</i>	<i>98CH40</i>	<i>01CH05</i>	<i>01CH05</i>	<i>01CH34</i>	<i>01CH34</i>	I	II	I	II	<i>98CH25d</i>	<i>01CH10</i>	<i>01CH10</i>	<i>01CH10</i>
SiO ₂	30,24	30,16	29,65	37,66	36,90	37,72	37,66	37,66	36,27	37,85					
TiO ₂	38,12	37,04	38,14	0,02	0,12	0,18	0,10	0,03	0,37						
Al ₂ O ₃	0,94	1,48	1,53	23,13	21,43	27,74	24,90	21,39	26,92						
Fe ₂ O ₃	1,46	1,44	0,20	0,01	0,00	0,09	0,05	0,03	0,03						
MnO	0,01	0,00	0,01	13,29	14,61	7,80	11,38	14,76	8,68						
CaO	28,83	28,36	29,15	0,23	0,24	0,31	0,10	2,23	0,26						
F	0,21	0,33	0,21	23,76	24,25	24,19	24,23	20,24	23,15						
H ₂ O ¹⁾	0,23	0,27	0,18	3,76	3,66	3,77	3,76	3,63	3,78						
Sum ²⁾	100,50	99,08	99,07	101,86	101,21	101,80	102,18	98,58	101,04						
Si	0,986	0,991	0,972	3,000	3,000	3,000	3,000	3,000	3,000						
Ti	0,934	0,915	0,940	2,172	2,054	2,601	2,338	2,0854	2,514						
Al	0,036	0,057	0,059	0,001	0,000	0,006	0,003	0,0017	0,002						
Fe ³⁺	0,036	0,036	0,005	0,797	0,894	0,467	0,682	0,9186	0,517						
Ca	1,007	0,998	1,024	0,014	0,015	0,019	0,006	0,1401	0,016						
Mn	0,000	0,000	0,000	0,001	0,007	0,011	0,006	0,002	0,022						
F	0,020	0,033	0,021	2,028	2,113	2,062	2,068	1,7931	1,965						
OH	0,050	0,058	0,040	2,000	2,000	2,000	2,000	2,000	2,000						
O*	4,921	4,907	4,913												

The proportions of cations are based on a normalization of Si to 3 cations; ¹⁾ value calculated; F, Cl are at detection limit; ²⁾ sum corrected for amount of F; O* = [(Σ positive valencies)-OH-F]/2
nd not determined; Cl below detection limit

Table 1 continued

	White Mica		Fe-Meta- Metapsammopelitic Garnet						Eastern Series			
	<i>Blueschist</i>		<i>Greenschist</i>		<i>sediment Schist</i>		<i>Mica-schist</i>		<i>Mica-schist</i>		<i>Granite</i>	
	98CH05	98CH05	01CH34	01CH34	98CH25	98CH33	98CH33	01CH10	01CH10	01CH29	01CH43	98CH43
	I	II	I	II	I	I	II	I	II	<i>Bt-zone</i>	<i>Stau-zone</i>	
SiO ₂	51,20	49,86	47,66	46,21	47,16	48,97	47,07	49,89	48,16	44,36	45,37	45,09
TiO ₂	0,06	0,06	0,23	0,26	0,04	0,19	3,44	0,08	0,33	0,16	0,25	0,16
Al ₂ O ₃	22,40	22,87	28,61	29,32	25,11	30,14	29,33	28,06	30,26	36,17	37,50	35,56
Cr ₂ O ₃	0,20	0,35	0,05	0,14	0,02	0,03	0,00	0,03	0,07	0,00	0,05	0,00
FeO	4,59	5,24	3,18	3,21	6,73	1,97	1,94	2,69	2,31	1,27	1,25	1,36
MnO	0,01	0,05	0,01	0,03	0,09	0,02	0,02	0,01	0,02	0,01	0,03	0,12
MgO	4,57	5,12	2,97	2,90	2,94	2,55	2,18	3,02	2,50	0,45	0,26	0,57
CaO	0,21	0,00	0,00	0,00	0,02	0,00	0,01	0,00	0,00	0,00	0,00	0,00
BaO	0,35	0,32	0,35	0,60	1,70	0,26	0,20	0,61	0,41	0,31	0,30	0,17
Na ₂ O	0,31	0,11	0,22	0,23	0,25	0,29	0,33	0,40	0,92	1,18	1,77	0,48
K ₂ O	10,53	10,40	10,94	10,74	10,23	10,43	10,64	10,23	9,63	9,92	8,51	10,06
H ₂ O ¹⁾	4,38	4,42	4,39	4,37	4,31	4,42	4,44	4,45	4,46	4,42	4,53	4,37
Sum	98,91	99,33	98,61	98,01	98,99	99,36	99,600	99,47	99,07	98,26	99,82	97,94
Si	7,003	6,764	6,503	6,347	6,569	6,550	6,334	6,703	6,480	6,023	6,173	6,094
Al ^{IV}	0,997	1,236	1,497	1,653	1,431	1,450	1,666	1,297	1,520	1,977	1,827	1,906
Al ^{VI}	2,614	2,421	3,104	3,092	2,690	3,300	2,986	3,146	3,279	3,811	3,694	3,759
Cr	0,022	0,038	0,005	0,015	0,002	0,003	0,348	0,004	0,007	0,000	0,000	0,000
Ti	0,006	0,006	0,023	0,027	0,004	0,019	0,000	0,008	0,034	0,017	0,013	0,016
Fe ²⁺	0,426	0,046	0,241	0,109	0,348	0,220	0,218	0,302	0,260	0,145	0,185	0,154
Fe ³⁺	0,099	0,549	0,122	0,260	0,436	0,000	0,000	0,000	0,000	0,000	0,000	0,000
Mn	0,002	0,005	0,001	0,004	0,010	0,003	0,002	0,001	0,002	0,002	0,009	0,014
Mg	0,931	1,036	0,604	0,594	0,610	0,509	0,437	0,604	0,502	0,092	0,153	0,115
Sum	4,100	4,100	4,100	4,100	4,100	4,054	3,992	4,065	4,084	4,066	4,054	4,058
Ca	0,031	0,000	0,000	0,000	0,003	0,000	0,001	0,000	0,000	0,000	0,000	0,000
Ba	0,019	0,017	0,019	0,032	0,093	0,014	0,010	0,032	0,022	0,016	0,007	0,009
Na	0,081	0,029	0,057	0,062	0,067	0,075	0,086	0,105	0,240	0,311	0,099	0,126
K	1,837	1,799	1,905	1,882	1,818	1,780	1,827	1,753	1,653	1,719	1,707	1,734
Sum	1,968	1,845	1,981	1,976	1,980	1,869	1,924	1,890	1,914	2,046	1,812	1,869
OH	4,000	4,000	4,000	4,000	4,000	4,000	4,000	4,000	4,000	4,000	4,000	4,000

The proportion of cations is based on 42 valencies neglecting the interlayer cations; the sum of octahedrally coordinated cations is set at 4.1 to allow for an estimation of Fe³⁺; the amounts of Cl and F are near or below detection limit; ¹⁾ amount calculated

	Chlorite		Blueschist		Greenschist		Ferruginous		Garnet		Metapsammopelite	
	<i>01CH05</i>		<i>01CH34</i>		<i>Metasediment</i>		<i>Mica-schist</i>		<i>98CH33</i>		<i>Mica-schist</i>	
	I	II	I	II	98CH25	01CH10	I	II	98CH33	I	II	01CH29
SiO ₂	27,23	27,05	26,39	26,73	27,39	25,70	26,27	25,91	25,56			
TiO ₂	0,06	0,00	0,05	0,04	0,01	0,00	0,05	0,03	0,10			
Al ₂ O ₃	18,92	19,30	21,14	20,92	19,42	14,84	21,30	21,61	19,32			
FeO	23,15	21,80	18,03	17,87	18,16	25,86	22,97	23,51	32,29			
MnO	0,27	0,33	0,17	0,13	1,55	0,48	0,37	0,41	0,24			
MgO	16,85	17,96	21,25	21,24	19,79	20,45	15,66	15,98	10,27			
H ₂ O ¹⁾	11,38	11,44	11,75	11,75	11,55	11,29	11,43	11,48	10,97			
Sum	97,86	97,88	98,78	98,68	97,87	98,62	98,05	98,93	98,75			
Si	5,740	5,670	5,386	5,455	5,662	5,457	2,755	2,707	2,795			
Al ^{IV}	2,260	2,331	2,614	2,545	2,338	2,544	1,389	1,368	1,205			
Al ^{VI}	2,440	2,437	2,469	2,486	2,412	2,574	2,015	2,055	1,285			
Ti	0,009	0,000	0,008	0,006	0,002	0,000	0,004	0,003	0,009			
Fe	4,082	3,822	3,077	3,049	3,151	4,591	2,015	2,055	2,952			
Mn	0,048	0,059	0,030	0,022	0,272	0,086	0,033	0,037	0,023			
Mg	5,295	5,611	6,464	6,460	6,120	4,697	2,448	2,489	1,673			
OH	16,000	16,000	16,000	16,000	16,000	16,000	16,000	16,000	16,000			

Cations based on 56 valencies; ¹⁾ value calculated; F, Cl are at detection limit;

Table 1 continued

Ferruginou											
Amphibole		S						Biotite			
Blueschist		Greenschist		Metasediment		Eastern Series		Stau-And		Kfs-Crd-Grt-	
98CH05	98CH05	01CH34	01CH34	98CH25	98CH25	Biotite-Zone	Zone	Sil-Zone			
I	II	I	II	I	II	01CH29		01CH43	01CH48		
SiO ₂	56,30	53,64	50,57	54,29	50,33	54,14	SiO ₂	33,15	33,74	33,91	
TiO ₂	0,04	0,02	0,19	0,03	0,03	0,03	TiO ₂	1,65	1,80	3,44	
Al ₂ O ₃	6,09	2,53	7,17	3,22	7,36	1,95	Al ₂ O ₃	18,33	19,47	19,04	
Cr ₂ O ₃	0,05	0,04	0,08	0,01	0,01	0,03	FeO	24,92	25,19	21,20	
Fe ₂ O ₃ ¹	6,11	3,05	4,82	3,20	11,07	7,51	MnO	0,14	0,07	0,05	
FeO	9,02	10,37	7,22	7,30	8,49	4,89	MgO	6,77	5,80	7,89	
MnO	0,14	0,28	0,32	0,28	0,99	1,40	CaO	0,00	0,02	0,00	
MgO	10,88	14,04	14,42	16,79	9,47	16,12	BaO	0,00	0,14	0,31	
CaO	2,58	9,08	10,25	11,39	4,32	9,61	Na ₂ O	0,04	0,31	0,35	
BaO	0,04	0,02	0,00	0,08	0,09	0,06	K ₂ O	8,73	8,62	9,32	
Na ₂ O	5,93	2,07	1,92	1,02	5,33	1,87	F	0,00	0,00	0,31	
K ₂ O	0,03	0,40	0,17	0,06	0,15	0,09	Cl	0,00	0,20	0,03	
H ₂ O ¹	2,12	2,01	2,06	2,09	2,06	2,11	H ₂ O ¹	3,76	3,73	3,73	
Sum ²	99,33	97,55	99,19	99,76	99,70	99,81	Sum ²	97,49	99,09	99,47	
Si	7,954	7,853	7,252	7,680	7,318	7,698	Si	5,289	5,293	5,232	
Al ^t	0,046	0,147	0,748	0,320	0,682	0,302	Al ^t	2,711	2,707	2,768	
Al ^o	0,968	0,290	0,464	0,218	0,579	0,024	Al ^o	0,737	0,894	0,694	
Ti	0,004	0,003	0,020	0,003	0,003	0,003	Ti	0,198	0,212	0,399	
Cr	0,005	0,004	0,009	0,001	0,001	0,003	Fe ²⁺	3,325	3,306	2,735	
Fe ³⁺	0,650	0,337	0,520	0,341	1,212	0,804	Mn	0,019	0,009	0,007	
Fe ²⁺	1,066	1,269	0,866	0,863	1,032	0,582	Mg	1,610	1,355	1,814	
Mn	0,017	0,034	0,038	0,034	0,122	0,169	Sum	5,888	5,776	5,649	
Mg	2,290	3,064	3,082	3,540	2,052	3,415	Ba	0,000	0,009	0,019	
Ca	0,390	1,424	1,575	1,727	0,672	1,464	Na	0,013	0,095	0,104	
Ba	0,002	0,001	0,000	0,005	0,005	0,004	K	1,777	1,726	1,834	
Na	1,623	0,587	0,533	0,280	1,516	0,515	Sum	1,790	1,830	1,956	
K	0,006	0,075	0,032	0,011	0,028	0,016	Cl	0,001	0,000	0,009	
Sum	2,022	2,087	2,139	2,022	2,208	1,998	F	0,000	0,097	0,153	
OH	2,000	2,000	2,000	2,000	2,000	2,000	OH	3,999	3,903	3,838	

The proportion of cations is based on 46 valencies and the sum of cations = 13 except for Ca, Na and K for estimation of Fe³⁺

Cations based on 44 valencies; ¹⁾ value Calculated; ²⁾ sum corrected for F and Cl

Table 1 continued

	Stilpnomelane	Staurolite		Cordierite
	<i>Fe-Metasediment</i>	<i>Mica-schist</i>		<i>Gneiss</i>
	98CH25	95CH29	98CH49	01CH48
SiO ₂	37,04	26,71	26,05	47,06
TiO ₂	0,01	0,48	0,40	0,02
Al ₂ O ₃	15,13	53,83	55,88	32,42
ZnO	0,01	0,29	0,01	
FeO	14,94	15,22	13,35	10,05
MnO	1,34	0,29	0,23	0,15
MgO	14,03	1,34	1,52	7,30
CaO	0,09			0,00
BaO	0,09			0,08
Na ₂ O	0,63			0,34
K ₂ O	4,48			0,01
H ₂ O ¹⁾	5,36	1,05	1,05	
Sum	93,15	99,21	98,49	97,43
Si	6,213	3,816	3,708	4,948
Al ^{IV}	2,787	0,184	0,292	1,052
Al ^{VI}	0,204	8,881	9,083	2,964
Ti	0,001	0,052	0,001	0,002
Zn	0,001	0,030	0,043	0,000
Fe ²⁺	0,164	1,819	1,590	0,883
Fe ³⁺	1,932	0,000	0,000	0,000
Mn	0,190	0,035	0,027	0,014
Mg	3,507	0,286	0,322	1,145
Sum	6,000	11,104	11,066	5,007
Ca	0,016	Cations based on		0,001
Ba	0,006	47 valencies		0,003
Na	0,204			0,069
K	0,959			0,001
Sum	1,185			0,073
				Cations
OH	6,000			based on
Cations based on 47.375 valencies neglecting				36
K+Na; Fe ³⁺ is estimated assuming 15 cations				valencies

Table 2 References for thermodynamic data and activity models used for the different geothermobarometric approaches

<u>Mineral</u>	<u>Components</u>	<u>End member data</u>	<u>Activity</u>
formulation			
For calculation of the pseudosections			
Clinopyroxene	jadeite, diopside, hedenbergite	Holland & Powell (1998a)	Vinograd (2002 a,b)
Na-amphibole	omphacite glaucophane, tremolite, tschermakite	Holland & Powell (1998a)	Will et al. (1998)
Ca-amphibole	Fe-glaucophane glaucophane, tremolite, tschermakite	Holland & Powell (1998a)	Dale et al. (2000)
Paragonite	Fe-actinolite, pargasite paragonite, margarite	Holland & Powell (1998a)	Will et al. (1998)
K-white mica	Fe-Al-celadonite, paragonite muscovite, Mg-Al-celadonite,	Holland & Powell (1998a)	Powell et al. (1999)
Biotite	annite, phlogopite, eastonite, ordered biotite	Holland & Powell (1998a)	Powell et al. (1999)
Chlorite	clinocllore, daphnite, Mg-amesite	Holland & Powell (1998a)	Holland & Powell (1998b)
Plagioclase	Al-free chlorite anorthite, albite	Holland & Powell (1998a)	Will et al. (1998)
Epidote	clinozoisite, epidote, Fe-epidote	Holland & Powell (1998a)	
Rutile, titanite, quartz		Holland & Powell (1998a)	a = 1
Magnetite, Lawsonite, K-Feldspar			
For calculation of the multivariant reactions			
Method 1			
Amphibole (1995a,b)	glaucophane	Evans (1990)	Massonne
(1995a,b)	tremolite	Berman (1988)	Massonne
Chlorite (1995a)	clinocllore	Massonne (1995b)	Massonne
(1995a)	daphnite	Massonne & Szpurka (1997)	as Massonne
Epidote	clinozoisite	Berman (1988)	$a_{\text{Clinozoisite}} = 1$
$X_{\text{Pistazite}}$			
Garnet	grossular	Berman (1990)	Berman (1990)
	pyrope	Berman (1990)	Berman (1990)
	almandine	Berman (1990)	Berman (1990)
K- white mica	muscovite	Massonne & Szpurka (1997)	Massonne 1997
	Mg-Al-celadonite	Massonne 1997	Massonne
(1995b, 1997)	Fe-Al-celadonite	Massonne (1995b)	Massonne
(1995b, 1997)	phlogopite	Berman (1988)	McMullin et al.
Biotite (1991)	Annite	Berman (1990)	McMullin et al.
(1991)			
Pumpellyite	Mg-pumpellyite	Evans (1990)	Evans (1990)
Stilpnomelane	stilpnomelane	Massonne & Szpurka (1997)	Massonne &
Szpurka (1997)			
Plagioclase	albite	Berman (1988)	$a_{\text{albite}} = X_{\text{albite}}$
Quartz		Berman (1988)	
K-feldspar		Berman (1988)	
Method 2			
Chlorite	clinocllore	Vidal et al. 2001	
	daphnite	Vidal et al. 2001	
	Mg-amesite	Vidal et al. 2001	
K- white mica	muscovite	Parra et al. 2002	
	Mg-Al-celadonite	Parra et al. 2002	
	Fe-Al-celadonite	Parra et al. 2002	

Table 3 List of calculated multivariant reactions

-
- (E1) $6 \text{ clinozoisite}_{\text{ep}} + 7 \text{ quartz} + 11 \text{ glaucophane}_{\text{amp}} + 10 \text{ Fe-Al-celadonite}_{\text{wm}} = 22 \text{ albite} + 3 \text{ Mg-Al-celadonite}_{\text{wm}} + 2 \text{ daphnite}_{\text{chl}} + 7 \text{ muscovite}_{\text{wm}} + 6 \text{ tremolite}_{\text{amp}}$
- (E2) $6 \text{ clinozoisite}_{\text{ep}} + 7 \text{ quartz} + 11 \text{ glaucophane}_{\text{amp}} + 7 \text{ Mg-Al-celadonite}_{\text{wm}} = 22 \text{ albite} + 2 \text{ clinocllore}_{\text{chl}} + 7 \text{ muscovite}_{\text{wm}} + 6 \text{ tremolite}_{\text{amp}}$
- (E3) $\text{daphnite}_{\text{chl}} + 5 \text{ Mg-Al-celadonite}_{\text{wm}} = 5 \text{ Fe-Al-celadonite}_{\text{wm}} + \text{clinocllore}_{\text{chl}}$
- (E4) $30 \text{ clinozoisite}_{\text{ep}} + 35 \text{ quartz} + 55 \text{ glaucophane}_{\text{amp}} + 35 \text{ Fe-Al-celadonite}_{\text{wm}} = 110 \text{ albite} + 7 \text{ daphnite}_{\text{chl}} + 3 \text{ clinocllore}_{\text{chl}} + 35 \text{ muscovite}_{\text{wm}} + 30 \text{ tremolite}_{\text{amp}}$
- (E5) $6 \text{ clinozoisite}_{\text{ep}} + 7 \text{ quartz} + 7 \text{ glaucophane}_{\text{amp}} + 9 \text{ Mg-Al-celadonite}_{\text{wm}} = 14 \text{ albite} + 9 \text{ muscovite}_{\text{wm}} + 6 \text{ tremolite}_{\text{amp}} + 4 \text{ H}_2\text{O}$
- (E6) $6 \text{ clinozoisite}_{\text{ep}} + 7 \text{ quartz} + 25 \text{ glaucophane}_{\text{amp}} + 14 \text{ H}_2\text{O} = 50 \text{ albite} + 9 \text{ clinocllore}_{\text{chl}} + 6 \text{ tremolite}_{\text{amp}}$
- (E7) $4 \text{ Mg-Al-celadonite}_{\text{wm}} + \text{daphnite}_{\text{chl}} + \text{muscovite}_{\text{wm}} = \text{Mg-amesite}_{\text{chl}} + 5 \text{ Fe-Al-celadonite}_{\text{wm}}$
- (E8) $5 \text{ Fe-Al-celadonite}_{\text{wm}} + 5 \text{ Mg-amesite}_{\text{chl}} = 5 \text{ muscovite}_{\text{wm}} + 4 \text{ clinocllore}_{\text{chl}} + \text{daphnite}_{\text{chl}}$
- (E9) $\text{Mg-Al-celadonite}_{\text{wm}} + \text{Mg-amesite}_{\text{chl}} = \text{muscovite}_{\text{wm}} + \text{clinocllore}_{\text{chl}}$
- (E10) $\text{clinocllore}_{\text{chl}} + 4 \text{ Al-celadonite}_{\text{wm}} = \text{muscovite}_{\text{wm}} + 3 \text{ phlogopite}_{\text{bt}} + 7 \text{ quartz} + 4 \text{ H}_2\text{O}$
- (E11) $3 \text{ Mg-Al-celadonite}_{\text{wm}} = \text{phlogopite}_{\text{bt}} + 2 \text{ K-feldspar} + 3 \text{ quartz} + 2 \text{ H}_2\text{O}$
- (E12) $\text{phlogopite}_{\text{bt}} + \text{almandine}_{\text{grt}} = \text{annite}_{\text{bt}} + \text{pyrope}_{\text{grt}}$
- (E13) $\text{pyrope}_{\text{grt}} + \text{grossular}_{\text{grt}} + \text{muscovite}_{\text{wm}} = 3 \text{ anorthite}_{\text{pl}} + \text{phlogopite}_{\text{bt}}$
- (E14) $\text{almandine}_{\text{grt}} + \text{grossular}_{\text{grt}} + \text{muscovite}_{\text{wm}} = 3 \text{ anorthite}_{\text{pl}} + \text{annite}_{\text{bt}}$
- (E15) $\text{grossular}_{\text{grt}} + \text{quartz} + 2 \text{ sillimanite} = 2 \text{ anorthite}_{\text{pl}}$
- (E16) $2 \text{ almandine}_{\text{grt}} + 2 \text{ phlogopite}_{\text{bt}} + 5 \text{ quartz} + 4 \text{ sillimanite} = 3 \text{ Mg-cordierite}_{\text{crd}} + 2 \text{ annite}_{\text{bt}}$
- (E17) $2 \text{ pyrope}_{\text{grt}} + 5 \text{ quartz} + 4 \text{ sillimanite} = 3 \text{ Mg-cordierite}_{\text{crd}}$
- (E18) $2 \text{ almandine}_{\text{grt}} + 6 \text{ anorthite}_{\text{pl}} + 2 \text{ phlogopite}_{\text{bt}} + 3 \text{ quartz} = 3 \text{ Mg-cordierite}_{\text{crd}} + 2 \text{ grossular}_{\text{grt}} + 2 \text{ annite}_{\text{bt}}$
- (E19) $3 \text{ Mg-cordierite}_{\text{crd}} + 5 \text{ grossular}_{\text{grt}} + 4 \text{ sillimanite} = 2 \text{ pyrope}_{\text{grt}} + 15 \text{ anorthite}_{\text{pl}}$
- (E20) $6 \text{ anorthite}_{\text{pl}} + 2 \text{ pyrope}_{\text{grt}} + 3 \text{ quartz} = 2 \text{ grossular}_{\text{grt}} + 3 \text{ Mg-cordierite}_{\text{crd}}$